2011

Characterization of biocompatible parylene-C coating for BioMEMS applications

Quoc Phuc Nguyen
Louisiana State University and Agricultural and Mechanical College

CHARACTERIZATION OF BIOCOMPATIBLE PARYLENE-C COATINGS FOR BIOMEMS APPLICATIONS

A Thesis

Submitted to the Graduate Faculty of the
Louisiana State University and
Agricultural and Mechanical College
in partial fulfillment of the
requirements for the degree of
Master of Science in Biological and Agricultural Engineering

in

The Department of Biological and Agricultural Engineering

by
Quoc Phuc Nguyen
B.S., Louisiana State University, 2007
December 2011

ACKNOWLEDGMENTS

This thesis was created through the efforts of committee members composed of Dr. Varshni Singh, Dr. Jost Goettert, and Dr. William Monroe. Funding was provided by the Louisiana Board of Regents and the Center for Advanced Microstructures and Devices (CAMD). Further thanks to Paratronix, Inc and Specialty Coating System (SCS) for providing parylene-C samples, CAMD's Microfabrication Group, Center for BioModular Multi-Scale Systems (CBM^2), Jennifer de Guzman and Dr. Robin McCarley (LSU Chemistry), Dr. Orhan Kizilkaya (CAMD), Dr. Eizi Morikawa (CAMD), Martina Cihova (CAMD/ Karlsruhe Institute of Technology, Germany), Dr. Proyag Datta, Dr. Todd Monroe's Lab, and departmental staff of Biological and Agricultural Engineering (BAE).

TABLE OF CONTENTS

LIST OF TABLES

LIST OF FIGURES

ABSTRACT

This thesis characterizes parylene-C films with respect to biological micro-electro-mechanical system (BioMEMS) applications. BioMEMS devices have fueled the growth and research in the area of detecting, analyzing and identifying pathogens rapidly with precision in the bio-medical applications, thereby positively impacting millions of lives and made it extremely popular among researchers. These devices are fabricated using state-of-the-art techniques usually involving more than one material which typically has different biocompatibility and is not acceptable for various BioMEMS and biomedical applications; therefore, a special biocompatible coating is required. The parylene polymer is an example of such a coating as it is known for its biocompatibility (U.S. Pharmacopoeia (USP) Class VI) as well as possessing pinhole free surfaces with low penetrability which provide exceptional barriers to moistures and solvents. The vapor deposition process utilized for depositing parylene coating also provide conformable, uniform thickness throughout targeted sample even with high aspect ratio microstructures, and is compatible with both polymeric (e.g. PMMA, polycarbonate, etc.) and non-polymeric (e.g. nickel, silicon, etc.) substrates, as the samples are kept inside a room temperature (25° C) chamber where the final deposition step occurs. In this study, parylene coatings were characterized with respect to surface roughness, where roughness measurements show no significantly changes when parylene are deposited on "smoother" pristine PMMA (from ~R_a=2.66nm to ~R_a=2.85nm) and polycarbonate (from ~R_a=3.02nm to ~R_a=5.92nm) and reduces roughness of "rougher" surfaces (electroplated nickel from ~R_a=374nm to ~R_a=201nm). Parylene is also characterize with respect to surface energy by measuring contact angles, where pristine parylene surface (contact angle = ~89°) becomes more hydrophilic by treating it with oxygen plasma (contact angle = ~32°). Surface modification was used to control the number of live cells (HeLa) attaching on parylene, where O_2 plasma was used to increase this by 2-folds and altering substrate roughness helped in minimizing the cells adhesion to parylene.

CHAPTER 1: INTRODUCTION

With the turn of the 21st Century, the miniaturization of the biological devices, an area of research known as Biological Micro-Electro-Mechanical Systems (BioMEMS), has become immensely popular due to its ability for rapid, accurate diagnostic results while requiring an exponentially lower sample volume by means of packaging the functionalities of large laboratory settings into small-scaled systems such as that of a lab-on-a-chip[1]. The concepts for these systems are to function as a small-scale replica of traditional laboratory settings which are small enough to be utilizable on-site. These BioMEMS can improve our everyday living from already existing devices, such as the easiness of home pregnancy test[2] or lower volume blood analysis cartridge system[3], to possible devices that can preemptively check for signs of osteoporosis[4] within minutes or on-site testing of water and air quality of high inquiry areas such as near nuclear and fossil fuel power plants, farmland runoffs, waste disposable sites, etc. Such devices like those mentioned above where size ranges from handheld to bench top, requiring low volume of samples (milliliters), and providing results within several minutes with acceptable accuracy are effective for their respective applications; however, other application such as bio-device for testing blood glucose level demands quicker results with high accuracy as minutes if not seconds are precious for saving patients with diabetes from suffering a coma.

The ever growing demands for more functionalities and/or higher efficiency and throughput can be met by high aspect ratio microstructures (HARMS)[5] and surface modification/ functionalization. Higher height to width aspect ratio allows greater number of structures to be fabricated within an area which provides tighter packages of devices and further reduces BioMEMS sizes. Furthermore, HARMS increase the surface area of devices beyond levels obtained from normal aspect ratio structures which allows for higher throughput. In addition, modification of surface energy and roughness of HARMS can functionalize the device by tailoring the aforementioned parameters to promote and/ or prevent

cells/proteins adhesion[6, 7]. For example, HARMS in devices used for biochemical applications such as micromixers, microreactors, and DNA concentrators[8] allows for more simultaneous solute-solvent interactions by providing higher surface area per unit volume thereby increasing the overall reaction rates. The innovative design of HARMS also provide tighter packaging and further increases efficiency in other devices such as DNA separators[9] and nanowell-plates[10], where more DNA separating post-like HARMS or wells can be added within an area. These BioMEMS devices are also more environmentally friendly and cost effective as they require by order of 2 to 3-folds less quantity of reagents/ chemicals/ samples and therefore producing a lower amount of overall bio and/or chemical hazardous waste. The strength of miniaturization and the inclusion of HARMS as highlighted by the given examples are beneficial for BioMEMS; however, the fabrication of these devices using the state-of-the-art microfabrication technology usually involve more than one material which is not acceptable to biological researchers 5, [11], thereby limiting their utilities.

The biocompatibility and material surface properties of the device are of utmost importance to researchers in the area of BioMEMS since they are typically working with several parameters such as device's bio- or chemical compatibility, uncontrolled protein adsorption, cells adhesion, and varying surface porosity and roughness. In order to not add any extra parameters, these bio-researchers ideally yearn for devices of a single material surface that will have minimum interactions or reactions with the sample and/or chemical involved. An optimal solution is to deposit a biocompatible coating on these miniaturized devices with HARMS and therefore allowing samples and/or chemicals to interact with only the coating surface, which should have desired properties such as conformability, lack of pinholes, chemical inertness, high dielectric strength, thermally stable, etc. Parylene, traditionally known in MEMS for possessing barrier property, is such a coating which possesses all the above properties as well as being lightweight, transparent, tailorable surface properties, and many other that are favorable for various BioMEMS applications.

Therefore, in the present study parylene film will be deposited on different types of substrates typically used in BioMEMS applications and will be characterized with respect to conformability, pinhole free property, surface modification/roughness/morphology, and biocompatibility with respect to biological cells.

CHAPTER 2: REVIEW OF LITERATURE

Parylene is the common name for the polymer poly-para-xylylene which was first discovered in 1947 by Michael Mojzesz Szwarc, a chemist who noticed a thin, yellowish snakeskin-like deposit with exceptional inertness both physically and chemically while investigating individual chemical bonding strength of aliphatic carbon-hydrogen bonds between toluene and xylene[12, 13, 14]. Szwarc's method of using xylenes in as the based material for vacuum thermal deposition yielded only a small percentage of the polymer film and it wasn't until a few years later that William Franklin Gorham conducted a more efficient deposition of parylene by using the stable dimer, di-para-xylylene, as the raw material[13, 14]. Gorham observed that at temperatures above 550° C and pressure below one Torr, the dimer undergoes pyrolysis and cleaves into two para-xylylene monomers. These monomers can then settle on the substrate surface, normally kept at room temperature, and begin its chain growth polymerization process that leads to high molecular weight parylene of 2000-4000 units per chain length[13, 15]. Since it was discovered, research for this polymer has yielded many variations (e.g. type –N, -C, -D, HT, etc.)[14]. Parylene-N (Figure 1), the traditional parylene originally discovered by Szwarc, has highest dielectric strength and the most penetration factor and conformability amongst the types of parylene but slow deposition rate due to its low threshold temperature (40°C) compared to other parylene types. Parylene-C (Figure 1), having substituted a single chlorine substitution for one of its aromatic hydrogen, has a slightly lower conformability due to its higher molecular weight but possesses the best biocompatibility (FDA Class VI) as well as threshold temperature close to 90°C. Similar to type-C, Parylene-D (Figure 1) has two chlorine substitutions which provide excellent thermal stability (135°C) but lower biocompatibility and conformability. In comparison to previously mentioned parylene types, Parylene-HT (Figure 1), which has its alpha hydrogen at the N dimer replaced with fluorine, is the most thermally stable (up to 350°C) and best used for high temperature applications[14].

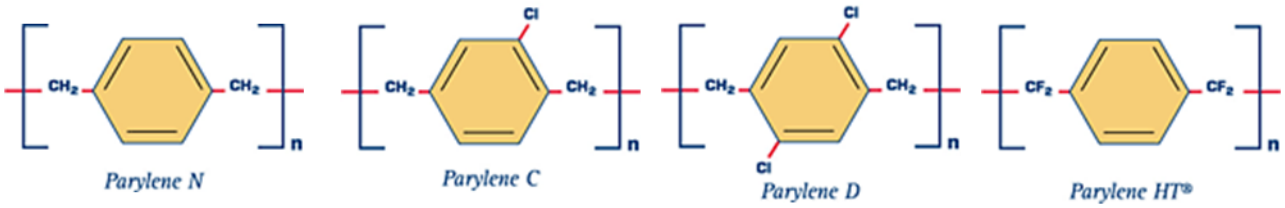

Figure 1: Molecular structures of some common types of parylene (-N, -C, -D, and HT).[14]

2.1 Parylene Properties

Parylene is known to possess many properties that are beneficial for BioMEMS applications. Specialty Coating Systems[14] and Fortin *et* Lu (2004)[13] have reported parylene coatings to be biocompatible, pinhole-free, conformable, and are great barriers against diffusion of moistures and gases as well as being chemically inert and resistant to acids and bases, thus providing excellent device protection against assaults from corrosion, bacteria and fungi. In addition, they documented thin film parylene being light weight, mechanically strong, and possesses low coefficient of friction and high dielectric strength which makes parylene suitable to be used as dielectric layers for coating sensitive electronic circuitry and MEMS devices. These properties of parylene and many others are shown below in Table 1.

Table 1: Various Properties of Parylene[14]

Properties	Parylene-N	Parylene-C	Parylene-D
Dielectric constant (1 MHz)	2.66	2.95	2.8
Dissipation factor (1 MHz)	0.001	0.013	0.002
Dielectric strength (MV/cm)	300	185-220	215
Volume resistivity (23°C, 50%RH, ω)	1.4×10^{17}	8.8×10^{16}	2×10^{16}
Surface resistivity (23°C, 50%RH, ω)	1×10^{13}	1×10^{14}	5×10^{16}
Melting point (°C)	420	290	380
Glass transition (°C)	13-80	35-80	110
Heat capacity (25°C, J/(gK))	1.3	1	-
Thermal conductivity (25°C, kW/(mK))	12	8.2	-
Density (g/cm^3)	1.11	1.289	1.418
Refractive index (in plane)	1.661	1.639	1.669
Tensile modulus (Gpa)	2.4	3.2	2.8
Tensile strength (MPa)	45	70	75

2.2 Surface Roughness and Cell Interactions

Cells interact with some material differently when they have different surface morphology at micro/nano level (surface roughness); therefore, studies of biological interactions with respect to surface roughness were conducted in order to understand and achieve better integration of cells *in vivo* [16, 17]. In Haberstroh *et al* (2003)[16] study, the authors mimic the nanometer roughness of native bladder tissue in order to enhance cellular responses. The authors used chemical etching procedures and casting methods to reduce surface feature dimensions of poly(lactic-co-glycolic acid) (PLGA) and poly(ether urethane) (PU) into nanometer regime. As seen in figure 2, the authors reported chemically processed nanometer features (~50-100nm) on PLGA surfaces and they observed that these surface had the highest bladder smooth muscle cell number adhering compared to conventional surfaces with roughness ~10-15µm, small micro-structured surfaces with roughness ~5-10um, and sub-micro structured surfaces with roughness ~100-1000nm. Moreover, the authors reported in Figure 2 that the number of smooth bladder cells adhering to the chemical treated nano-structured surface is a significant increase from the number of cells adhering to casting micro structured surfaces thus smooth bladder cells prefer PLGA surfaces with nano sized roughness within ~50-100nm over micro sized roughness of 10-15µm.

The results presented by the authors for PU are different from PLGA. The authors show in Figure 3, that nano structured PU surfaces (~50-100nm) have the lowest number of bladder smooth muscle cells adhesion. The authors also reported the number of cells on PU surface with micro-structured roughness is significantly higher than PU surface with nano-structured roughness which they explained that chemical changes to PU surface is a more influential factor than roughness.

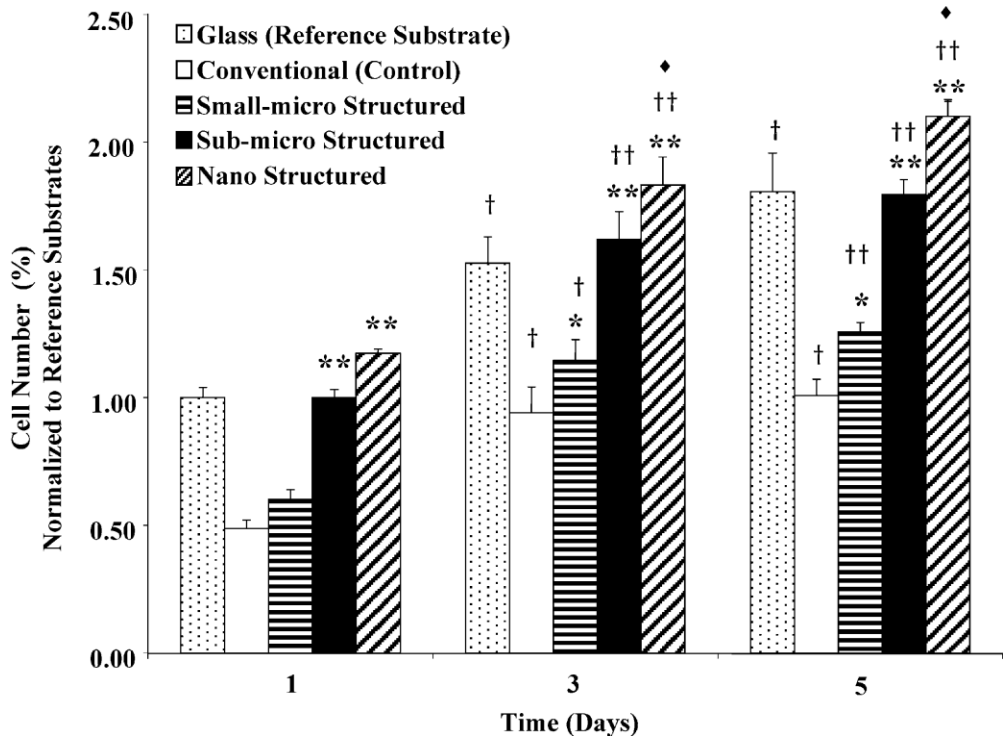

Figure 2: Graph shows chemically treated nano-structured PLGA has the highest number of cell adhesion and cells number significantly increases on surface with nano-structured roughness in comparison to surfaces with micro-structured roughness.[16]

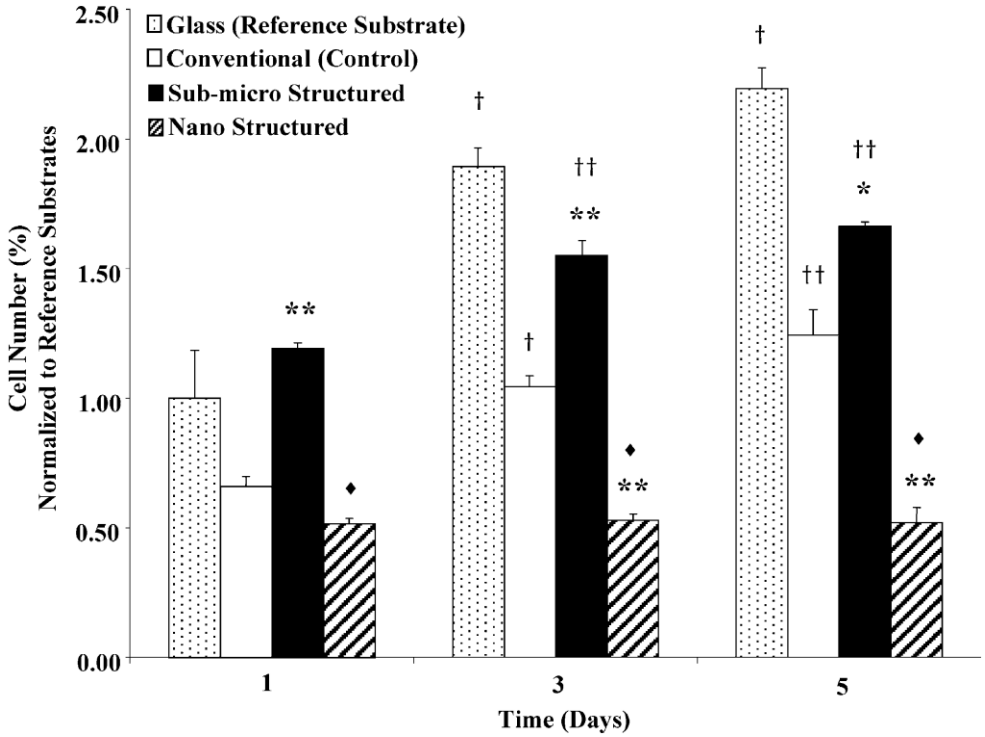

Figure 3: Graph shows chemically treated nano-structured PU has the lowest number of cell adhesion.[16]

In addition to using chemical techniques, the authors also reported using casting method to produce nano-structured features. In Figure 4, the authors presented results on PLGA that show higher number of cells on nano-structured surfaces than the micro-structured surfaces and glass samples. The authors stated that the results indicate that roughness play a more important role in cellular interactions than chemical processing for PLGA. Overall, Haberstroh *et al* (2003)[16] has shown that cells interact differently on the surfaces of PLGA and PU that are varying in surface roughness and surface chemistry. PLGA and PU with the same nano-roughness values have reverse effect on adhesion of smooth bladder cells.

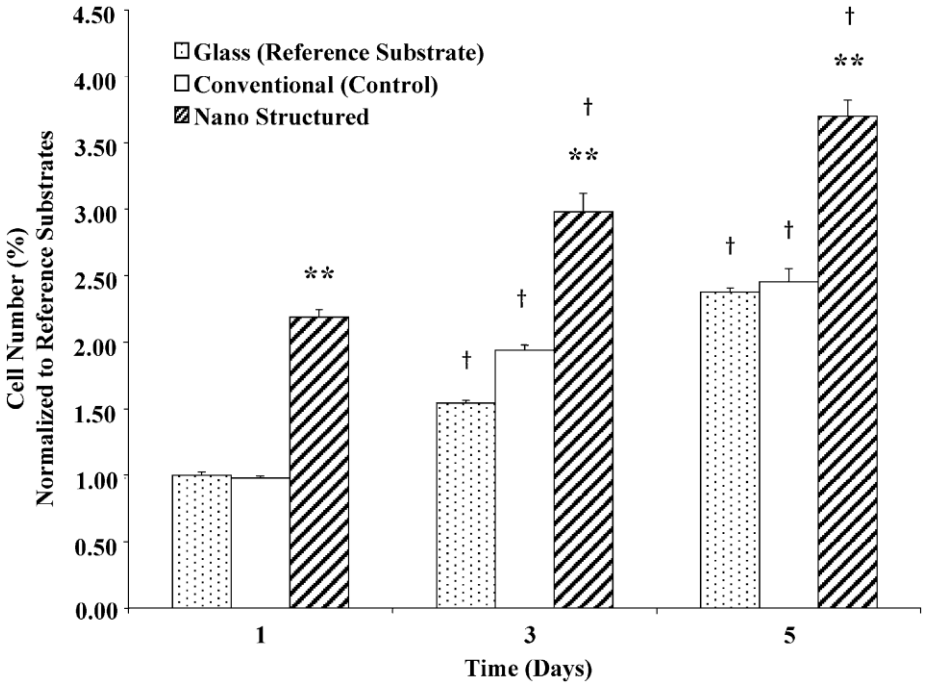

Figure 4: Graph shows chemically untreated nano-structured PLGA has the highest number of cells. Compared to chemically untreated micro-structured PLGA, the number of bladder smooth muscle cells was increased on chemically untreated nano-structured surface.[16]

2.3 Conformable Deposition of High Aspect Ratio Microstructures

Using the state-of-the-art technology, high aspect ratio microstructures (HARMS) may be fabricated from more than one material whereby a biocompatible coating is needed to conformably

deposit throughout the microstructures without significantly changing the structural dimensions. Noh *et al* (2004)[18] used a method dubbed by the authors as "parylene micromolding" that can effectively produce microfluidic channels at higher rate at lower cost. According to the authors, the traditional dry etching practices of parylene using RIE and DRIE to fabricate microfluidic channels call for a sacrificial photo-resist (PR) layer. The process, illustrated by the authors in Figure 5, begins with the first layer of parylene deposition to act as a foundation, Figure 5A. It is followed with a PR layer which acts as structural framework for the microfluidic channel, Figure 5C. Afterwards, another layer of parylene is deposit to form an enclosed microfluidic structures, Figure 5D. Subsequently, the top parylene layer is patterned to expose the sacrificial PR layer which is removed to form microfluidic channels, Figure 5E and 5F. Noh *et al* (2004)[18] noted that the conventional method is a slow process that may take several days to complete; especially the removal of PR layer which is a diffusion-dependent process at the solute-solvent interface and requires extra washing steps to remove excess PR.

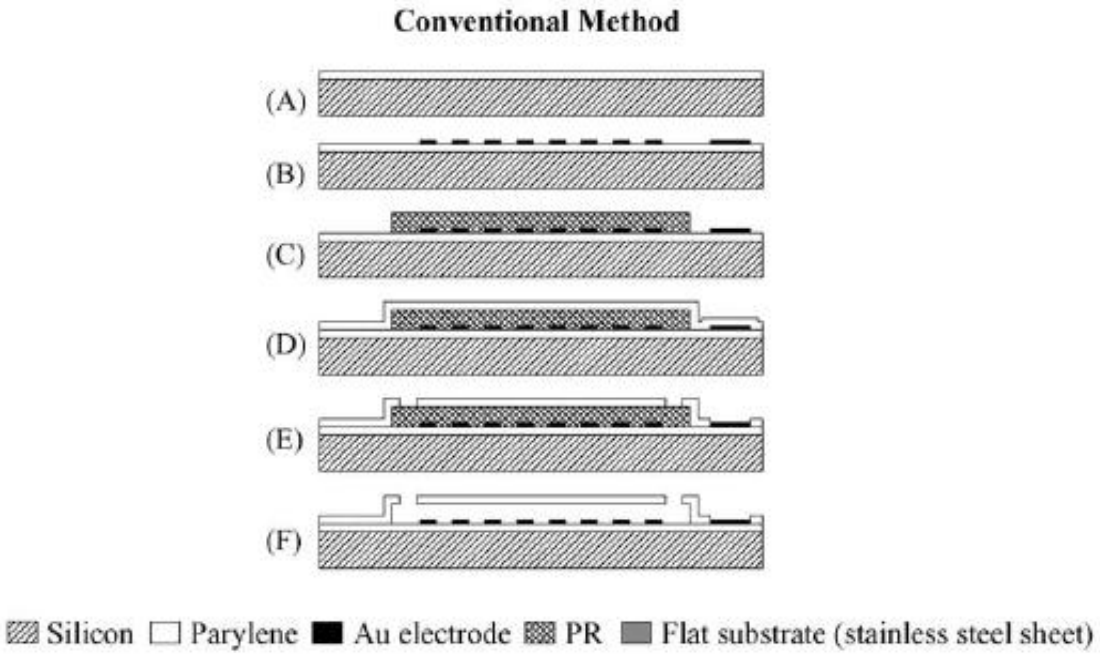

Figure 5: Fabrication of parylene microchannels using the conventional method involves A) parylene deposition, B) patterning of electrode, C) patterning of PR sacrificial layer, D) another parylene deposition, E) RIE patterning of parylene, and F) dissolution of PR layer. [18]

In contrast to conventional method, the micromolding process illustrated in Figure 6 begins with a mold with pre-fabricated microchannels, Figure 6A. Layers of parylene are then simultaneously deposited on the mold (Figure 6B) and a separate flat substrate (Figure 6C). Finally, the two parylene layers are bonded (Figure 6D) and the flat substrate is removed (Figure 6E) to complete the microfluidic structures (Figure 6F). Noh *et al* (2004)[18] asserted that parylene "micromolding" effectively reduced time and cost by abandoning the sacrificial PR layer and reducing the number of needed etching steps involved in the entire process.

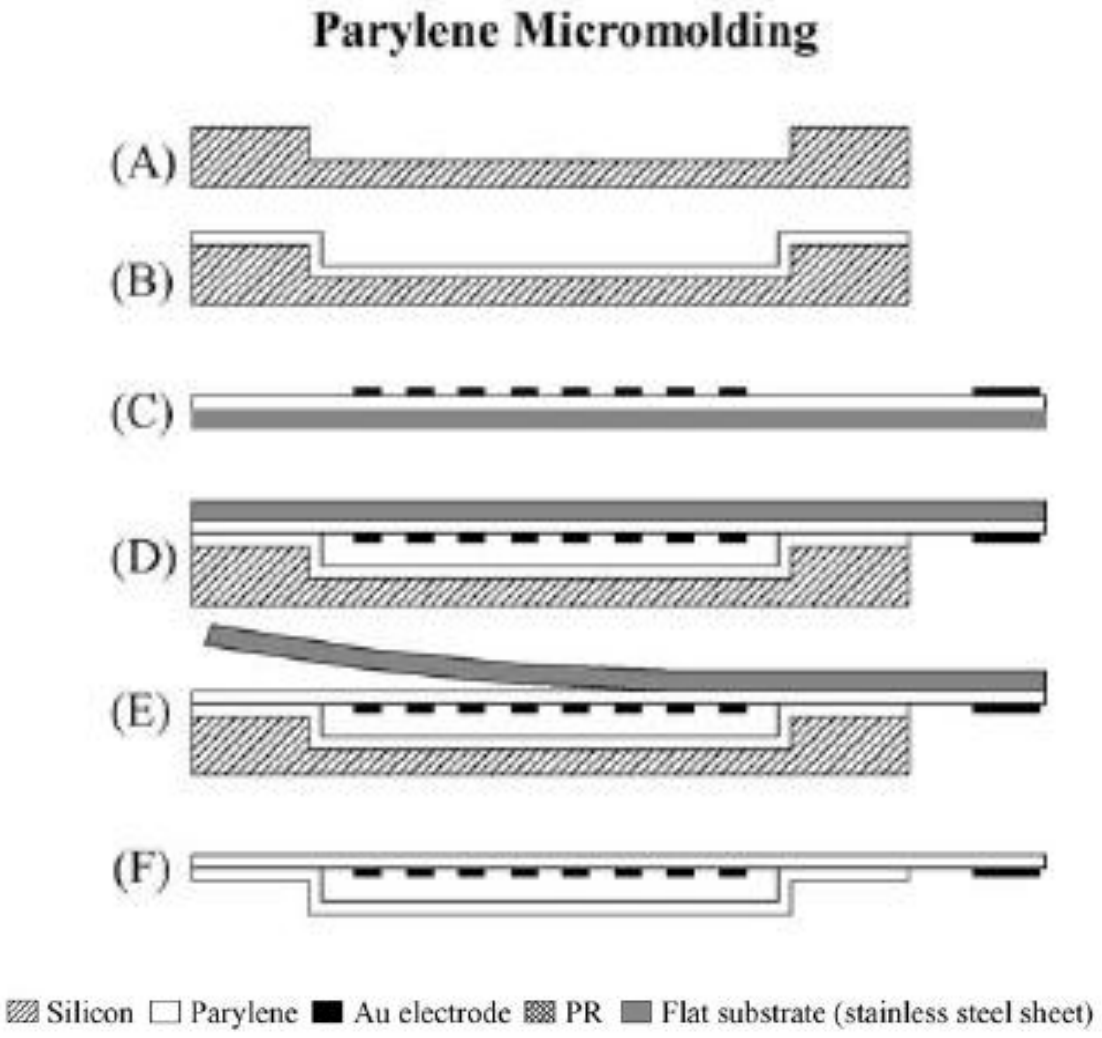

Figure 6: Fabrication of parylene microchannels using parylene micromolding involves A) using DRIE to produce Si mold, B) parylene deposition, C) deposition of parylene and patterning of electrode onto a flat substrate, D) thermal bonding, E) substrate removal, and F) KOH etching of Si mold.[18]

The authors' micromolding process added a bonding step, so they investigated several thermally stable flat substrates for parylene deposition such as glass, silicon, and different type of metals to find optimum bonding conditions. Their investigation resulted in an optimum bonding temperature above 190° C at 24 MPa of pressure. The authors also performed shear stress and leakage tests to evaluate the quality of the thermal bonding. As reported the shear strength of the bonded parylene structures was 2 MPa and no leakages were observed from the parylene microchannels at flow rate of less than 0.2 sccm. Noh *et al* (2004)[18] added that higher flow rates were not evaluated because the soft tubing used in the experiment as microfluidic interconnections failed at 0.2sccm.

The authors investigated conformability of parylene deposition by examining the uniformity of the coating. Noh *et al* (2004)[18] performed the analysis by depositing 10µm thick parylene onto silicon microfluidic structures of 100um width and 300um height (aspect ratio 3) and reported that parylene is conformably deposited with uniform thickness (Figure 7). However, they noted that the parylene film did adhere well to the silicon mold and de-bonded during the dicing process used to prepare the cross-section.

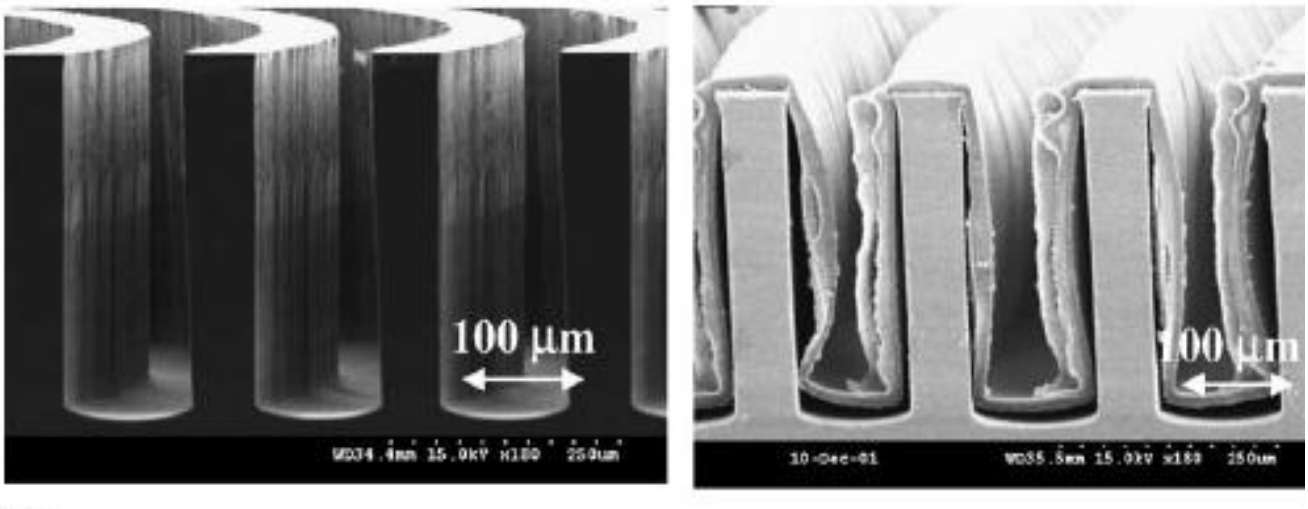

Figure 7: SEM images of silicon microchannels (100um deep and 300um wide) before (left) and after (right) 10um parylene deposition. [18]

Changes to sidewall surface roughness after parylene deposition were observed by Noh *et al* (2004)[18]. The authors showed in Figure 8, the Si microfluidic structure sidewalls before (left) deposition

has rough patterns that are produced from the etching process. These patterns appear to be smoother after (right) parylene deposition. Noh *et al* (2004)[18] only qualitatively observed the changes in surface roughness and attributed the smoother sidewalls seen after deposition to the thickness of 10um parylene being much larger than the roughness produced by the etching process.

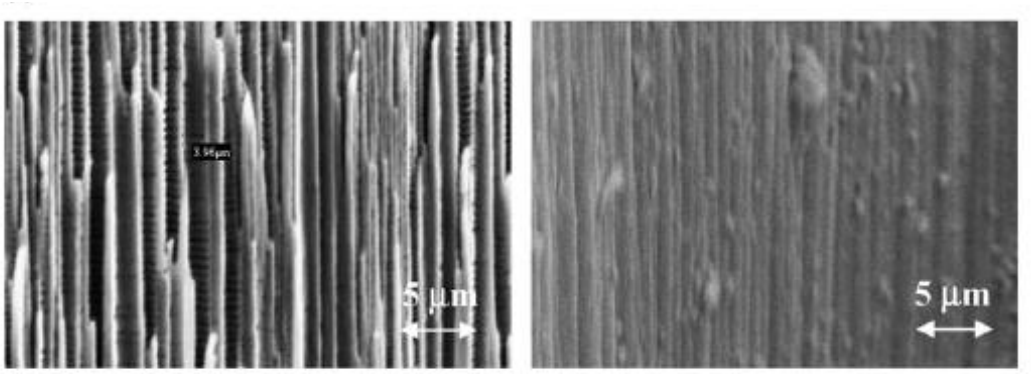

Figure 8: SEM images of Si microchannel sidewalls before (left) and after (right) parylene deposition. Smoother sidewall roughness was observed after deposition. [18]

In summary, Noh *et al* (2004)[18] had developed a more rapid and cost effective technique for fabrication of parylene microfluidic channel by utilizing the parylene deposition process and the authors reported that this process conformably coats HARMS with aspect ratio of 3. They also noticed reduction to sidewall roughness after deposition and qualitatively reported the comparison.

In addition to fabricating HARMS by depositing parylene on pre-fabricated structures, Youn *et al* (2007)[21] reported using parylene-C to fabricate micro patterned mold master through the combination of hot-embossing and electroplating techniques. The authors stated that the micro molds are generally fabricated from electroplating metals onto non-reusable Si substrates that are produced by a well-developed, very high cost, and timely micromachining process. The longevity for these micro-molds are usually short because they are repeatedly expose to embossing conditions such as unevenness of mold/samples, hard metallic dust particles, complexity of designs, and extreme embossing/releasing conditions[19], [20]. Therefore, Youn *et al* (2007)[21] reported a new method of using flexible parylene master mold that will enable easier release as well as replication of metallic micro molds without needed to

continuously micromachine master mold, Figure 9. The authors have used the following process which begins with parylene-C deposition onto a substrate. Then, they used a mold to hot-emboss microstructures onto the parylene-C. Afterwards, Youn *et al* (2007)[21] sputtered an initial seeding layer onto the parylene microstructures for the subsequent electroplating. Lastly, the authors planarized the newly electroplated structures and released the completed mold from the parylene. Using this method, the authors stated of achieving embossed microstructure profiles with <2.32% parameter deviations between mold and parylene, which is less than the <2.94% parameter deviations between mold and PMMA. The authors stated that more molds can then be fabricated by reusing the parylene mold masters for electroplating.

The parylene thickness deposited in this study is documented to be 60µm, which requires several depositions and can take several days to achieve. Additionally, the authors have demonstrated feasibility of the technique by using microstructures with aspect ratios of $\leq$ 2.5 for the molded structures, where aspect ratio of 10 can normally be achieve.

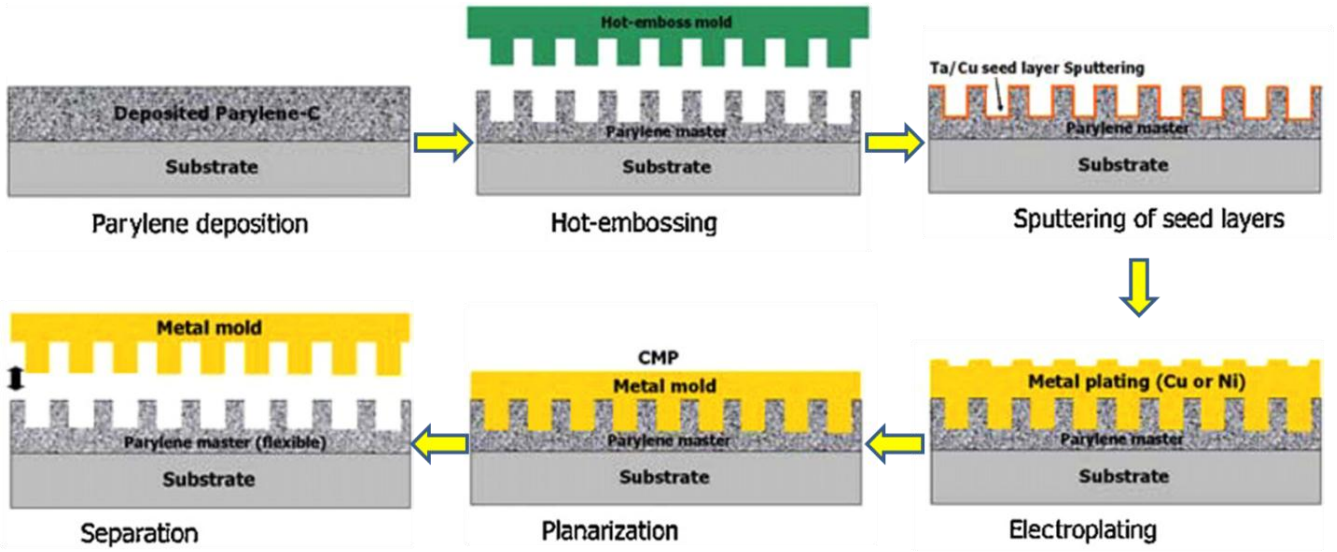

Figure 9: A schematic diagram showing the hot-embossing and electroplating process used to produce flexible parylene master molds. [21]

Kroschwitz (1998)[22] and Meng and Tai (2008)[12] have reported that parylene coating cannot be degraded hydrolytically which directly contribute to the polymer chemical inertness and resistances. Further, Meng and Tai (2008)[12] informed that this chemical inertness makes patterning parylene using wet

etching techniques impractical since studies conducted by Specialty Coating Systems reported only chloronapthelene and benzolyl benzoate can be use to dissolve parylene. However, the process requires temperature above 150°C which Meng and Tai (2008)[12] reported to not being compatible with common lithographic processes. As a more practical means of patterning parylene, Meng and Tai (2008) has published a study involving etching rates of parylene using dry methods such as reactive ion etching (RIE) and deep reactive ion etching (DRIE). The authors reported that DRIE provide the fastest removal rate of parylene at 0.77 um/min, followed by RIE at 0.56 um/min, and lastly plasma at 0.19 um/min. The authors also noted that etching rates of parylene in all three dry etching techniques are slower in comparison to the photo-resist, AZ4620. Details of the results are summarized in Table 2.

Table 2: Etching rates of parylene with respect to plasma, RIE, and DRIE in comparison to photoresist (AZ 4620) [12]

Etching Technique	Parylene	AZ 4620
Plasma (200mT, 400W)	.19 um/min	.29 um/min
RIE (100 sscm, 200mT, 400W	.56 um/min	.67um/min
DRIE (60 sscm, 23mT, 800W)	.77 um/min	.94 um/min

Meng and Tai (2008)[12] also noticed difference in etching profile between plasma, RIE, and DRIE (Figure 10). The authors observed that plasma etching produced samples that exhibit lateral etching and tapered profiles (Figure 10A). Meanwhile, they noted that RIE and DRIE etched structures produces nearly vertical sidewalls (Figure 10B and 10C). Meng and Tai (2008)[12] also added that parylene may be patterned using dry etching techniques with aspect ratio of 1:1 achieved using plasma and aspect ratio of 2:1 using RIE and DRIE.

2.4 Surface Modification and Cell Interactions

Surface modification can change the chemistry, roughness, and morphology of material surface which affects biological cells interactions. Feili *et al* (2005)7 performed cell growth study of parylene-C using mouse fibroblast (L 929) and the results show deposited parylene-C contribute no toxicity to the mouse

cell line. The authors qualitatively show in Figure 11 that cells adhering to pristine (left) parylene-C surface are morphologically rounder and are clustered as compared to oxygen (O_2) plasma modified (right) parylene-C surfaces. The scratch lines in the images indicate a division between surfaces of petri dishes and parylene-C.

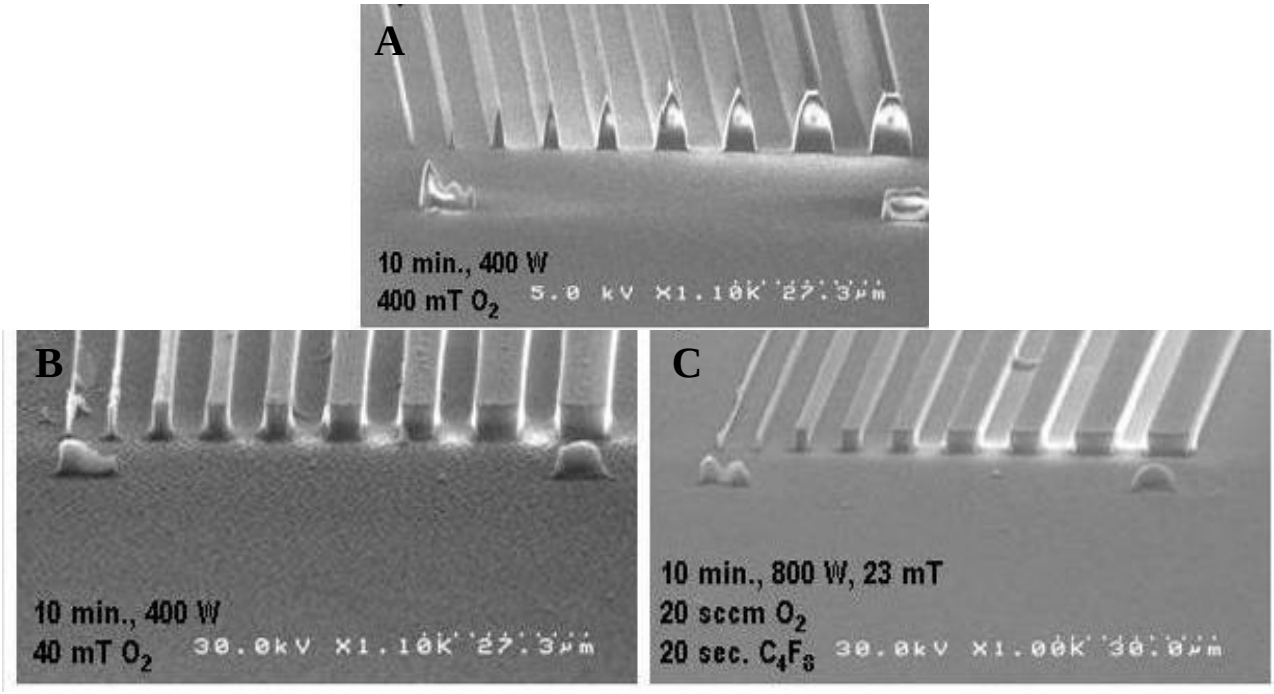

Figure 10: Etching profiles of parylene structures using A) plasma, B) RIE, C) and DRIE. [12]

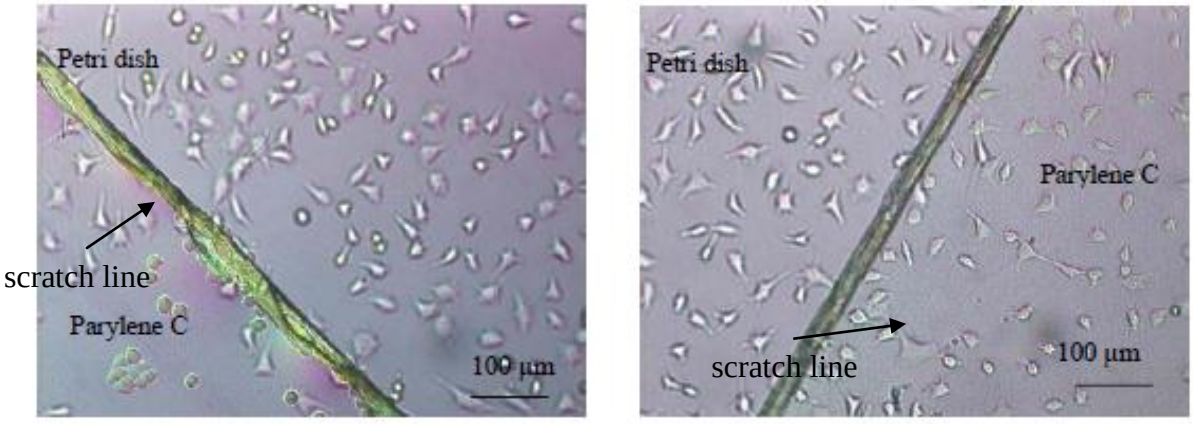

Figure 11: L-929 cells incubated on parylene surfaces. Left image shows viable but reduce number of cells on parylene compared to polystyrene. Right image shows an increase to viable cells after dry etching parylene with O_2.[7]

Chang *et al* (2007)[23] has also investigated cellular interaction between parylene-C surfaces and mammalian cell lines; NIH-3T3 fibroblasts and AML-12 hepatocytes. The results, as shown in Figure 12, obtained by the authors show NIH-3T3 fibroblasts do not adhere well to pristine parylene-C surfaces as the percentage of cells adhering to the surface with respect to loading density is below 40%. The figure also show NIH- 3T3 adhesion to the surface doubled to over 80% by functionalizing the substrates by oxygen plasma treatment or seeding with fibronectin (proteins) layer. The percentages between oxygen plasma treated or fibronectin-coated surfaces were very similar. NIH-3T3 does not adhere to pristine parylene-C. Cell adhesion is promoted by functionalizing parylene-C surface with oxygen plasma or protein coating.

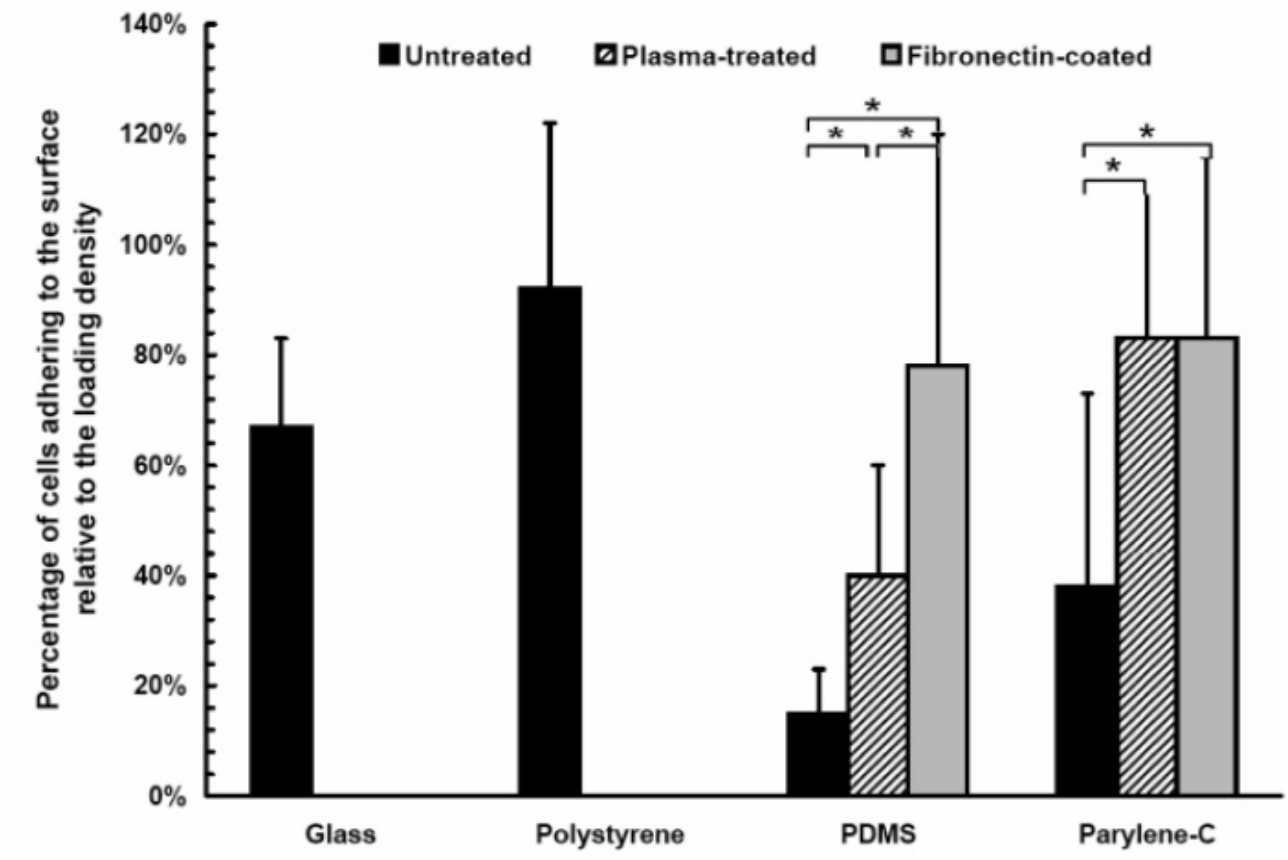

Figure 12: Chart displaying percentages of NIH-3T3 fibroblasts relative to loading density adhering to various pristine and functionalized surfaces. NIH-3T3 does not adhere to pristine parylene-C. Cell adhesion is promoted by functionalizing parylene-C surface with oxygen plasma or protein coating. [23]

Cell adhesion results for AML-12 hepatocytes were similar to NIH-3T3 fibroblasts as Figure 13 shows the percentage of adhering AML-12 on pristine parylene-C is below 5% and that percentage increases dramatically to about 60% and 70% when cultivated on oxygen plasma treated and fibronectin-coated parylene surfaces, respectively.

The authors also characterized the surface roughness of parylene-C using AFM. The measurements within a 50um x 50um scan area show pristine parylene-C to have average roughness (Ra) of 19.3 $\pm$ 6.3 nm. The roughness remains relatively unchanged after oxygen plasma treatment, Ra = 19.3 $\pm$ 5.4 nm. An increase to 29.0 $\pm$11.5 nm was measured on fibronectin coated parylene-C. The authors also measured contact angle (CA) for surface energy analysis and the results obtained show pristine parylene C having a CA of 97.2 $\pm$ 4.2 and that angle dramatically decrease to 4.4 $\pm$ 2.4 due to O_2 plasma.

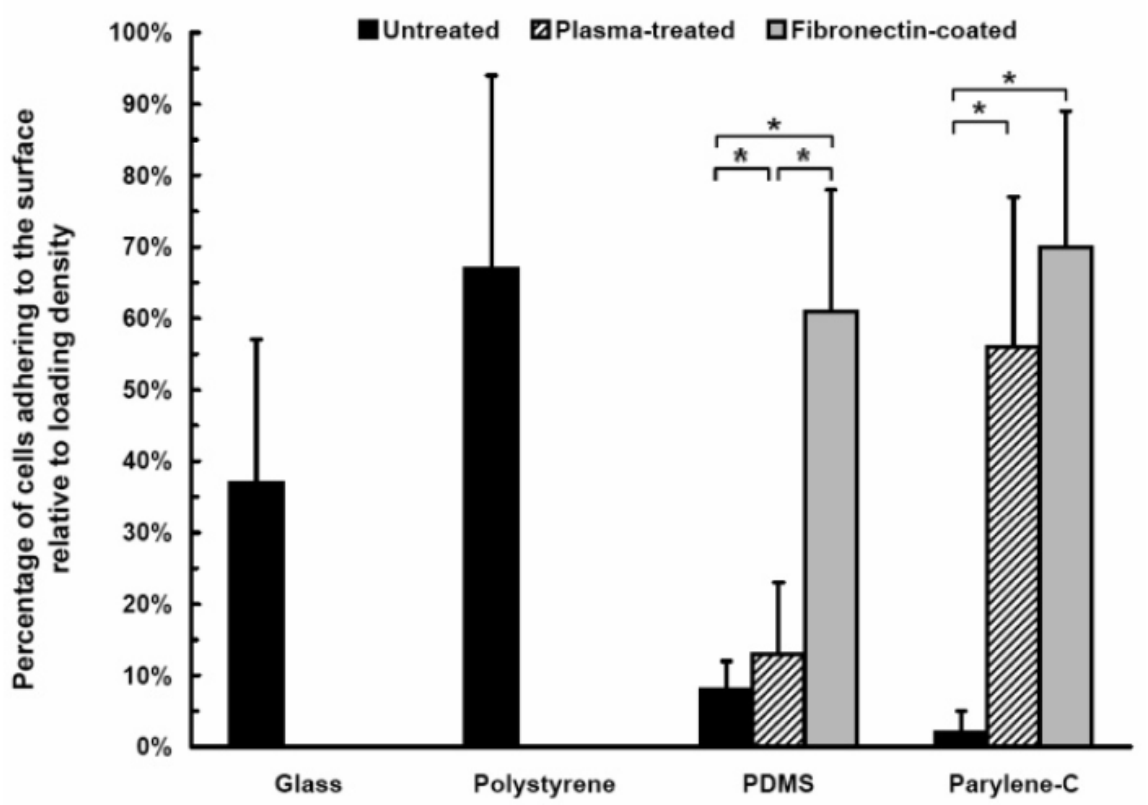

Figure 13: Chart displaying percentages of AML-12 hepatocytes relative to loading density adhering to various pristine and functionalized surfaces. AML-12 does not adhere to pristine parylene-C. Cell adhesion is promoted by functionalizing parylene-C surface with oxygen plasma or protein coating.[23]

2.5 Applications of Parylene

2.5.1 Cell and Protein Patterning

Studies have also been conducted to investigate the possibility of applying parylene coating as a mask layer for better controls of cell and protein adhesion. One method used is called the lift-off process. Wright *et al* (2007)[24] uses this method to create a reusable parylene membrane for patterning of NIH-3T3 fibroblasts, AML12 hepatocytes, and embryonic stem cells. The authors, illustrated in Figure 14, initiate the procedure by depositing parylene onto silicon substrate and then etched using oxygen plasma. Next, Wright et al (2007) apply the etched parylene stencils as a masking layer onto various substrates (e.g. PDMS, polystyrene, glass, and methacrylated glass). Subsequently, they patterned the substrate by incubating with solution containing cells/ proteins and washing off non-adhered solution. Finally, the authors remove, clean, and reuse the stencils. By following this method, the authors reported to be able to maintain pattern integrity with feature size >200um diameter using 10um thickness parylene stencils.

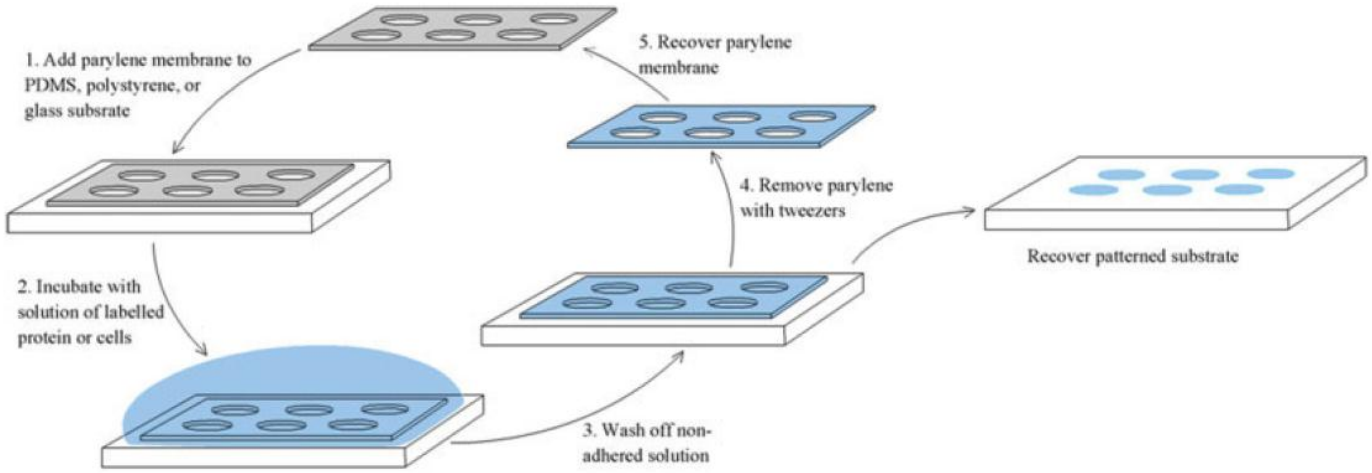

Figure 14: The lift-off process used by Wright *et al* (2007) to create a reusable parylene membrane for cell patterning. [24]

Ilic *et al* (2000)[25] also implemented a dry lift-off process using parylene to pattern Escherichia *coli* serotype O157:H7 onto many type of protein treated surfaces using poly-L-lysine and

aminopropyltriethoxysilane (APTS) SAMs, Figure 15. Ilic *et al* (2005) fabricated various topologies, such as spirals, dots, and lines onto silicon, pyrex, quartz, and alumina substrates to test the patterning of biological agents. The authors reported the parylene thickness used was just less than one micron and that the bacteria patterned were confined within stripes of parallel lines varying from 2um to 20um. Similarly, Atsuta *et al* (2007)[26] reported using parylene-C with 5um thickness as a masking layer for patterning of proteins using networks of microfluidic channels within PDMS.

The various lift-off studies discussed above have shown successful attempts at patterning cells and proteins by using parylene as a masking layer and further investigations into interactions between biological materials and parylene are needed. The biological materials did not directly interact with parylene but instead parylene was used as a masking layer which is later remove to reveal patterns of cells and proteins.

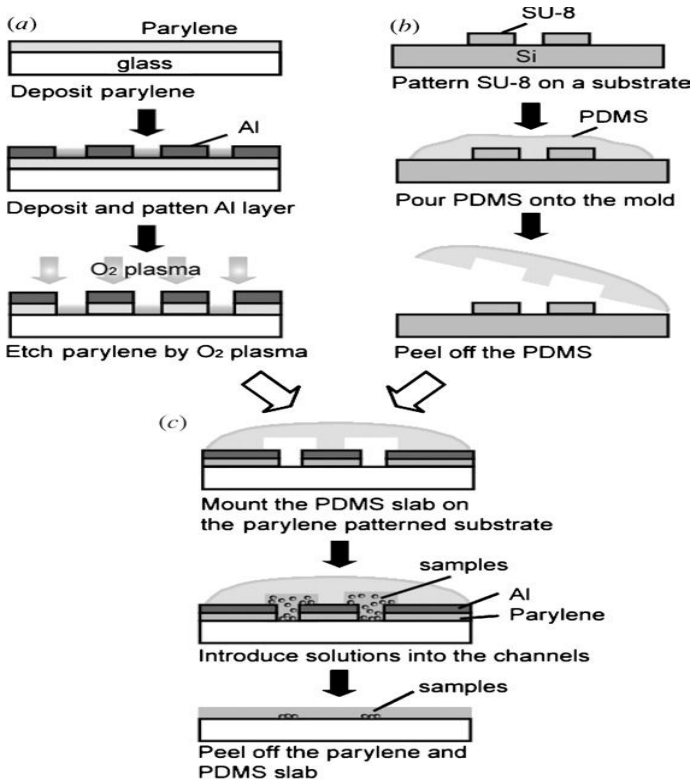

Figure 15: The wet lift-off process uses a parylene masking layer for patterning protein. The parylene mask is removed after patterning. [26]

CHAPTER 3: SPECIFIC AIMS AND OBJECTIVES

Overall, the objective of this Master Thesis is the characterization of parylene-C as a biocompatible coating for BioMEMS Devices. The specific focus of the study was on:

1. To study/investigate conformability, pinhole properties with respect to high aspect ratio microstructures.
2. To study/investigate the surface properties,
3. To tailor the surface roughness by varying the deposition parameters or modifying the surface physically
4. and to characterize these films with respect to interactions with live cells (HeLa).

CHAPTER 4: MATERIALS AND METHODS

Parylene was deposited on different types of samples and the surfaces were characterized using various techniques. In this chapter, I will discuss the details of depositing parylene and the parameters followed by the techniques employed to characterize the surfaces.

4.1 Deposition of Parylene Thin Films

Parylene is deposited using the chemical vapor deposition (CVD) technique. The CVD technique utilizes the vapor form of the monomer and introduces that into a deposition chamber where the monomers adsorb to the substrate surface and begin to polymerize at room temperature (Fortin and Lu 2004). This is significant as the CVD process enable deposition of parylene at room temperature as oppose to high temperature where it is incompatible with most polymer substrates due to polymer's inherent lower glass transitional temperature. Furthermore, unlike other deposition methods (e.g. dipping, spraying, or spin-on), CVD avoid an intermediate liquid stage thus producing uniform, smooth, stress-free coating that is able to penetrate crevices of any-shaped devices and deposited at room temperature (Fortin and Lu 2004). Parylene deposition process begins with the vaporization zone (Figure 16A), where solid dimers are vaporize (100-175°C, 1 torr). Then, gaseous dimers travel into the pyrolization zone (Figure 16B) and pyrolyze (~680°C, 0.5 torr) into monomers. Finally, monomers enter the deposition zone (Figure 16C), where samples are kept (room temperature, 0.1 torr), adhere to all surfaces (<40°C), and begin polymerize into parylene films.

4.2 Materials and Sample Preparations

The substrate materials used in this research included flat, non-structured surfaces as well as microfabricated HARMS composed of poly (methyl methacrylate) (PMMA), polycarbonate (PC), and nickel (Figure 17). Flat, non-structured polymeric samples were prepared by milling sheets of PMMA and PC into 20 mm by 20 mm square-shaped pieces, which are able to fit into 35mm diameter petri dishes.

Before parylene deposition, polymeric samples were cleaned inside a cleanroom environment by rinsing with deionized water and dried with dry nitrogen air. Nickel substrates were also cleaned in the same manner using isopropanol instead of deionized water. Cross-sections for SEM analyses were prepared by incasing parylene-coated samples using a resin and hardener (Buehler® Expoxicure™ Resin No. 20-8130, Buehler® Expoxicure™ Hardener No. 20-8132). After allowing the resin and hardener to dried, the preserved samples were manually polished (Hyprez® Lapping Systems) successively in 1µm slurry using 400 grit, 600 grit, 800 grit, and finally cloth papers. Cross sections were also obtained by dicing the samples using a dicing wheel cooled with cooling solution without mounting in resin.

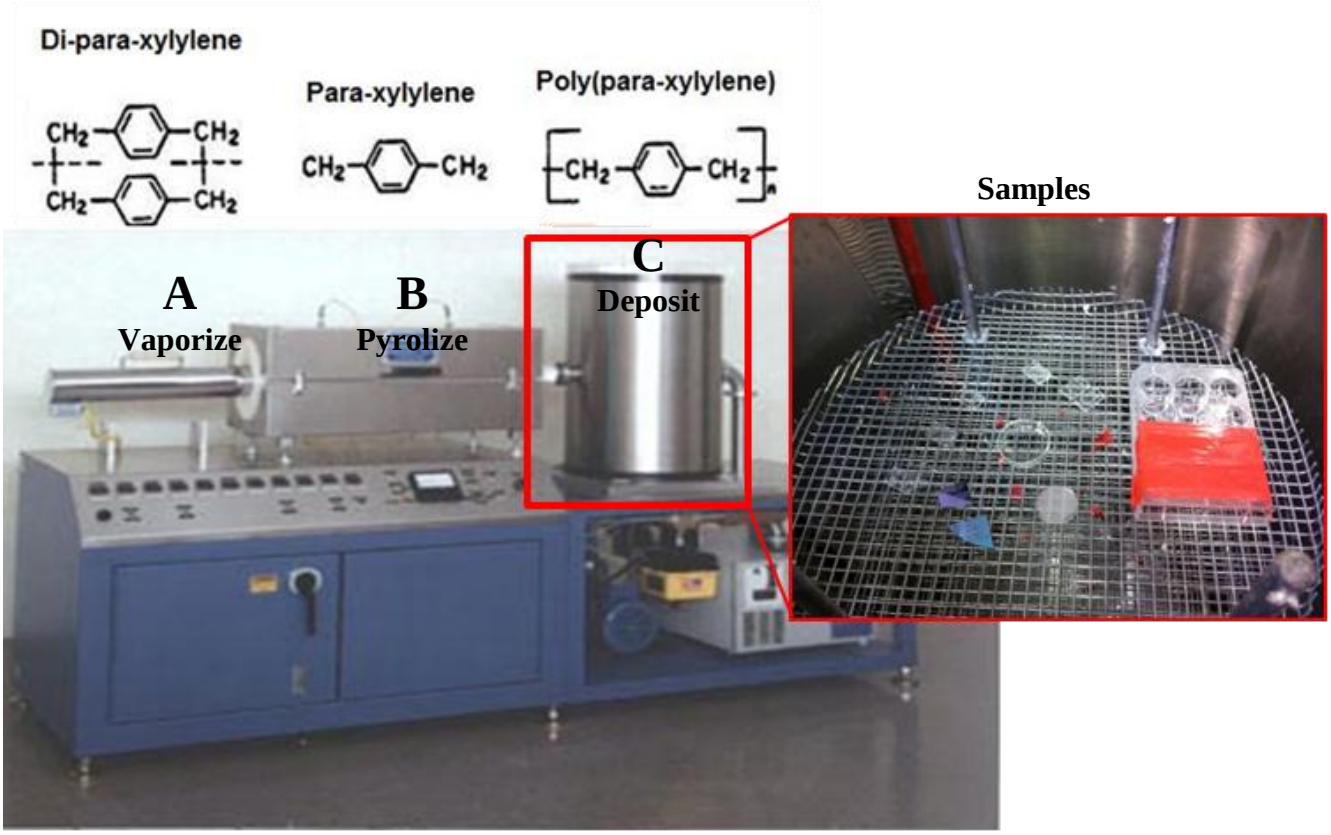

Figure 16: Deposition process system mainly composes of 3 stages: 1) vaporization, 2) pyrolysis, and 3) deposition. A) In the vaporization chamber, solid dimers are heated (~100-175° C, 1 mm Hg) until they vaporized into gases. B) The extreme temperature (~680° C, .5 mm Hg) within the pyrolysis chamber cleaves the gaseous dimers into monomers. C) Finally, the monomers deposit on substrates and polymerize at room temperature (25° C, .1 mm Hg) within the deposition chamber.[14]

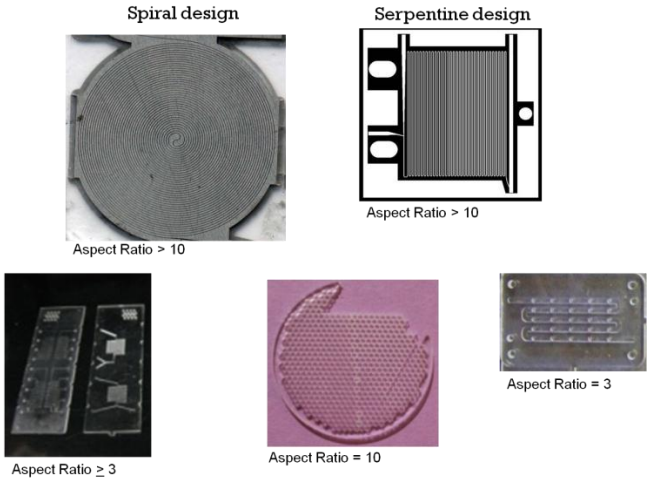

Figure 17: Examples of polymeric and metallic samples used in this study.

4.3 Surface Roughness Measurements

Surface roughness measurements were performed on pristine and surface modified substrates using an optical profiler (Wyko NT3300, Veeco) (Figure 18A) and atomic force microscopy (AFM) (Nanoscope IIIa, Digital Instruments, Veeco). Roughness measurements performed by optical profiler were done in vertical scanning interferometry (VSI) mode. In this mode the instrument has vertical resolution of 3nm and the spatial resolution depends on the combination of objective and aperture lens used. The measurement areas on the samples were randomly chosen and measured using 20X objective with a 0.5 field of view, which provide a scan area of 230 µm by 300 µm. In the AFM case which has resolution of ~0.3nm, roughness measurements were done in non-contact mode. In this mode, the cantilever freely oscillate at its resonance frequency without coming in contact with the sample surface and provide images of the oscillating force due to Van der Waals force or dipole-dipole interaction between the cantilever tips and sample surface. Locations for roughness measurement were randomly chosen on the sample with scan area of 50 um x 50 um for bulk surface analysis. Scan area of 5um x 5um were also conducted for higher resolution analysis to compare if any surface roughness profile changes at more localize area. At least three measurements, performed by optical profiler and AFM, were made on

each substrate, and at least 3 substrates were measured for each surface to obtained average root-mean-square (rms) values of roughness. Scanning electron microscope (SEM) (Figure 18B), which has magnification up to 500,000X and a resolution range of 4.0nm to 1.5nm, is also used to study the surface morphology as well as qualitatively analyzing and/or comparing the surface roughness. The analyses were conducted using SEM at low acceleration voltages from 1-5 KeV and 15-18mm working distance.

Figure 18: Analysis equipments: A) Vecco Wyko NT3300; B) Hitachi S-4500 II FESEM

4.4 Surface Modifications

PMMA, PC, and parylene-C surfaces were modified by exposing the surface to oxygen plasma (Branson Plasma Asher) at 600 W for three minutes. Surfaces were sterilized prior to cell adhesion study by soaking samples in 75% ethanol solution for 10 minutes and afterwards air dried within a cell culture hood. Effects of surface modification were investigated in the form of changing surface energy which can be correlated by analyzing contact angles. The contact angle (θ) is produce from the interfacial energy of the liquid-gas interface (γ_{LG}) and solid-liquid interface (γ_{SL}) and is defined by the Young's Equation:

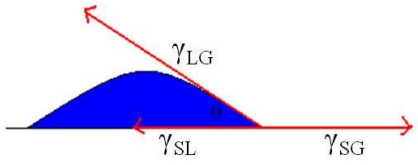

$$0 = \gamma_{LG} - \gamma_{SL} - \gamma cos\theta,$$

$\gamma_{LG} = surface\ energy\ at\ the\ liquid - gas\ interface$
$\gamma_{SL} = surface\ \ energy\ at\ the\ solid - liquid\ interface$
$\theta = contact\ angle$

Surfaces with $\theta < 90°$ are considered to be hydrophilic and those with $\theta \geq 90°$ are hydrophobic. A special case known as the Lotus effect is reserved for super hydrophobic surfaces of $\theta > 150°$. Measurements of the contact angle in this study were carry out using static drops of nano-pure water (2 μL) which were automatically dispensed by the surface analysis system (VCA Surface Analysis System with Optima XE software) (Figure 19), which has an automated calculation method for measuring $0 \leq \theta \leq 180$ with $\pm$ 0.5 degree accuracy and a repeatability of $\pm$1 degree. The measurements were conducted for surfaces of pristine, O_2 plasma-treated, 75% ethanol-sterilized, and plasma-EtOH samples, where at least three measurements were taken from randomly chosen locations on each substrate and repeated at least three times for statistical merit of average values.

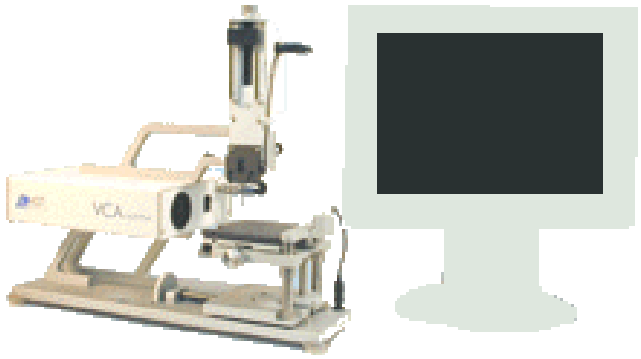

www.astp.com/vca/vca_optima.html

Figure 19: VCA Optima Surface Analysis System

4.5 Cell Adhesion

Biological characterization of parylene as deposited and surface modified was performed using HeLa cells. Biological interactions are examined using fluorescent spectroscopy and cell health indicator assay to evaluate cellular adhesion which can be use to analyze cytotoxicity, cell growth, and spreading and proliferation. HeLa epithelial cells were cultured in Dulbecoo's Modification of Eagle Medium (DMEM) in addition with 3% fetal bovine serum and maintained in an incubator at 37°C with 5% CO_2

atmosphere. In preparation for cell adhesion experiments, the HeLa cells were trysinized, counted using a haemocytometer, and re-suspended in DMEM + 3%FBS to form 10,000 cells/cm^2 with respect to 35mm petri dish stock solution. Three milliliters of the stock solution are dispense via micropipette onto sterilized samples with dimensions 2cm x 2cm (Figure 20), which were chosen because it fits within petri dishes with diameter of 35mm, and incubated for 6, 24, and 48 hours. Each substrate has a base area of 4 cm^2 which corresponds to ~40,000 cells/cm^2 loading density.

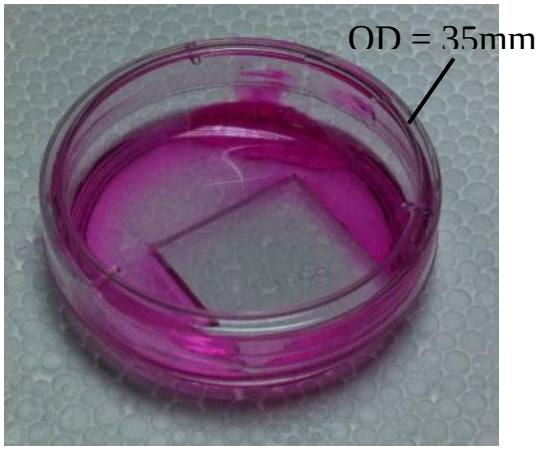

Figure 20: Cell adhesion setup. HeLa cells are cultured on substrates (PMMA, PC, parylene) are housed within a 35mm polystyrene dish and incubated for 6, 24, and 48 hours.

Fluorescent microscopy (Nikon Eclipse TE 1000 with a CCD camera) (Figure 21) was used to observe adhesion of cells on each surface. Fluorescent staining of live cells were performed using a viability assay (Calcein AM, Invitrogen™). Calcein AM (Figure 22) is stain which is use to measure cell viability and/or cytotoxicity as it is initially a non-fluorescent, hydrophobic compound that easily permeates intact, live cells and afterwards hydrolyzes by intracellular esterase to produce calcein, a hydrophilic, strongly fluorescent compound that is well-retained in the cytoplasm. HeLa cells are stained with 3uM Calcein AM and kept in an incubator for 30 minutes. Afterwards, the cells are rinsed with and kept in phosphate buffered saline (PBS) (Mg++, Ca++) and observe with fluorescent microscope using FITC filter set of excitation wavelength of 490 and emission wavelength of 520.

www.nikon-instruments.jp/eng/page/products/ts100.aspx

Figure 21: Fluorescent microscope use for imaging of HeLa cells in this study.

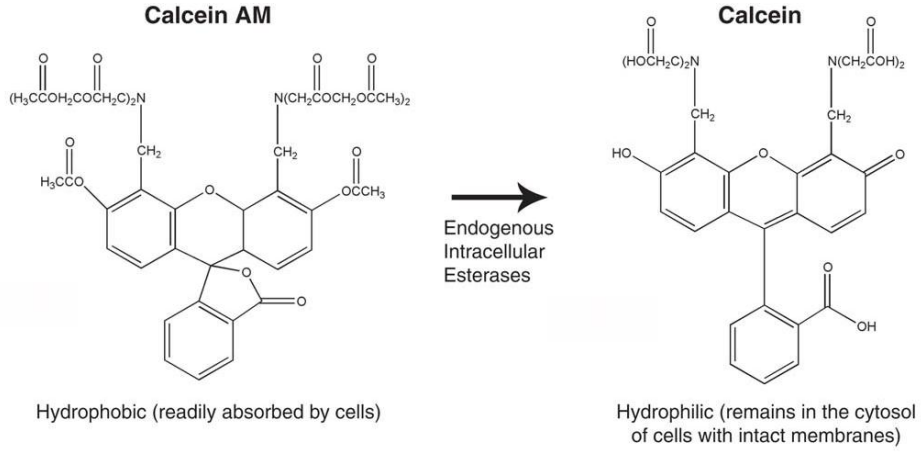

Figure 22: Molecular structures of non-fluorescent compound Calcein AM® and it's conversion to fluorescent compound calcein after being hydrolyzed by intercellular esterase.[14]

Cell health and proliferation analysis was performed using a cell health indicator assay (alamarBlue®, Invitrogen™). AlamarBlue® assay (Figure 23) contains a non-fluorescent indicator dye, resazurin, which is converted to bright red–fluorescent resorufin via the reduction reactions of metabolically active cells, and the amount of fluorescence produced is proportional to the number of living cells. The amount of alamarBlue® reagent added is equal to 10% volume of cell solution and stored

in an incubator for 2 hours. Hereafter, three 100uL volumes were pipette into 96-wells plate and readings were taken using a plate reader with 515/595 excitation/emission filter.

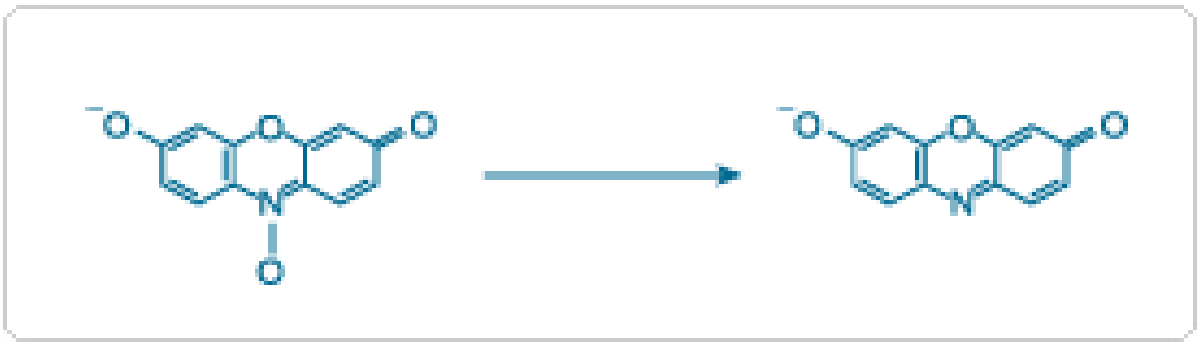

Figure 23: Molecular structure of resazurin, a non-fluorescent compound in alamarBlue® that is reduced to bright-fed fluorescent compound resorufin by metabolically active cells.[14]

CHAPTER 5: RESULTS AND DISCUSSIONS

Surface characterization using various techniques was performed on of different samples deposit with parylene. In this section, I will present and the discuss in details the results of surface characterization of parylene coating deposited on metallic and polymeric substrates with respect to conformability, pinhole-free coating, adhesion, surface roughness/ modification, and live cells study.

5.1 Conformable, Pinhole-Free Coating with Excellent Adhesion

The conformability of parylene-C coating was studied by examining the cross sections of parylene-deposited microstructures with aspect ratios (AR) ranging from 1:1 to 13:1. One micron thick parylene was deposited on these samples, and they were cross-sectioned by mounting as described in section 4.2. SEM micrographs in Figure 24 show the cross sections of Ni HARMS depth 500µm and width 45µm, where 1um parylene coating deposited on the HARMS is clearly seen. The red boxes in Figure 24A shows that the parylene coating is following the rough contour of the microchannels, which is clearly seen in the zoomed-in images, along the top (Figure 24B), the bottom (Figure 24C), and the sidewalls (Figures 24B and 24C) of the nickel HARMS. Further, the zoomed in images (Figure 24B and 24C) clearly show that parylene coating has uniform thickness of ~1µm all along the surfaces of the Ni channels. The conformability and uniformity achieved in parylene coating is as expected[13, 14] due its unique deposition process already discussed. The results show that parylene monomers at the 37mTorr vacuum level goes and freely adsorbed uniformly over the entire depth of the HARMS channels and then simultaneously polymerizes one molecule at a time[14] which is unlike other processes such as liquid or spray-on techniques that are more line-of-sights and cause bridging and pooling on microstructures[13]. Observations along the parylene-Ni interface, presented in Figures 24B and 24C, show parylene coating in complete contact with the nickel surfaces and no gaps, even down to micro-scaled as evident from SEM micrographs, are detected even after the polishing steps describe previously in section 4.2. Thereby,

it is evident that no de-bonding had occurred and good adhesion was achieved. The good adhesion is most likely due to parylene affinity to nickel and/or promoted by the surface roughness on the nickel substrates, which is further detailed in section 5.2. Similar results were observed in all the other channels that are spaced every 150um apart.

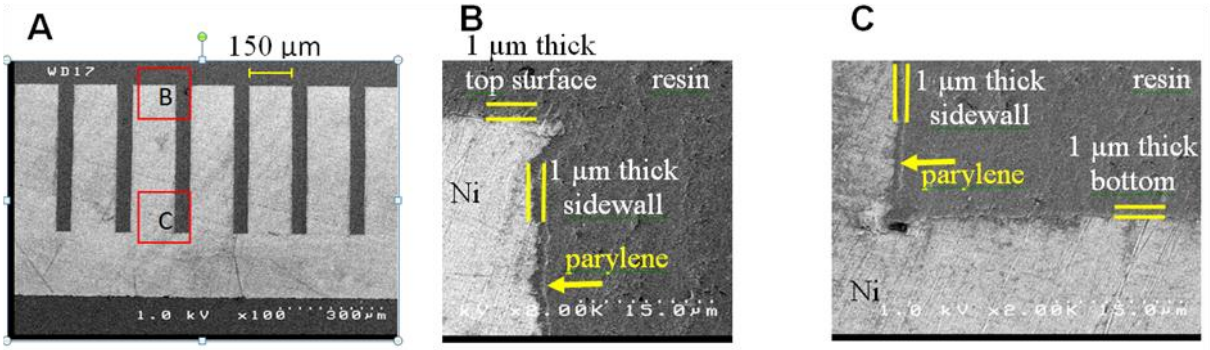

Figure 24: SEM images of cross-sectioned HARMS samples used to analyze quality of parylene deposition. A) A full view of a Ni HARM structure with channels 500um/45um depth/width and 150um spacing prepared by mounting and manual polishing. B) 2,000X magnification of the top of the Ni HARM showcasing uniform deposition of ~1um parylene along top surface and sidewall. C) 2,000X magnification of the bottom of the Ni HARM shows the same uniform thickness of ~1um along the bottom surface and sidewall.

Likewise, conformal deposition of parylene was also seen in polymeric substrates, polycarbonate and PMMA. However, the coating easily de-bonded (Figure 25) during dicing procedure describe in section 4.2. Dicing conditions were different for each sample, where slow cutting speed of 0.1-0.5µm/s were used for Ni substrates which allow enough time for parylene to also cut with minimal force, and faster cutting speed of 1-5µm/s were used for polymer substrates which may not allow adequate time for parylene to cut and also may add tensile forces between parylene and the polymers leading to debonding. In addition, these samples were also not mounted while dicing; therefore, lack the stress relieving hard resin interface. The debonding seen between parylene and PMMA substrate (Figure 25) is likely resulted from the dicing process. In comparison to the study previously mentioned in section 2.3, parylene was shown to have better adhesion to nickel than silicon substrates. The result is mostly likely due to differences in the procedures during sample preparation. Although they were not measured, the dicing forces used in the previous study[18] were possibly higher than the polishing forces used in this study,

which may explains the de-bonding and deformations observed by Noh *et al* (2004) at the parylene-silicon interface and those observed by this study at the parylene-PMMA interfaces. Mounting of the nickel HARMS sample in resin may have aid in achieving better bonding; however, the factor most likely is minute as small gaps will be apparent in SEM micrographs if any de-bonding have occurs regardless whether mounting was used or not.

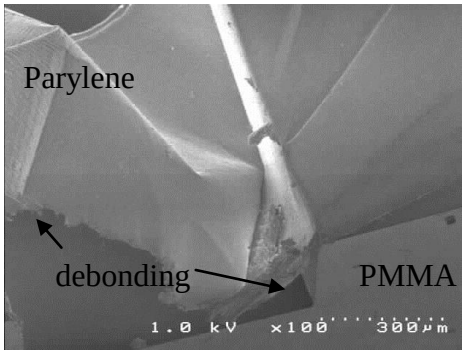

Figure 25: Cross section of PMMA sample obtained by dicing without mounting. Debonding can be seen at the parylene-PMMA interface.

In addition to conformable deposition, pinhole properties are also examined. Parylene film of thickness ~1µm was deposited on PMMA and the SEM micrographs shown in Figure 26 exhibit this coating as pinhole-free with respect to biological cell applications. High magnification SEM images (Figure 26A) and 4x zoom-in view [inset] show no pinholes down to $\geq$100nm diameter within the coating. Furthermore, higher resolution images (Figure 26B and 4x zoom-in [inset]), from mySEM® (NovelX) , a low voltage SEM that is able to image 3D surface morphology due to its quad detector, further present parylene-coated surface free of pinholes down to sub-10nm resolution. The lack of pinholes is most likely resulted from the single molecule chain growth of parylene during vapor deposition and the present work demonstrates that his mechanism is compatible with PMMA, PC, and Ni substrates. Although pinholes were not observed in any of the parylene coating, various sub-micron sized (~250-500nm) spots are present on the surface (Figure 26B). The size ranges, sparse distributions, and non-circular geometry of the spots indicate that they are likely to be defects that may have been introduced to the surface pre-

deposition as natural imperfections on the PMMA surface or dust particles or residues that attached to the sample surface during transportation from the cleanroom to the deposition chamber and/or inside the chamber before vacuum is achieved and subsequently conformably preserved during deposition. The non-circular geometry defect (Figure 26B inset) justifies it is not a pinhole as pinhole's are expected to be of well defined circular shape. These unwanted features may be minimized and/or avoided by having a deposition system inside a cleanroom. These kinds of defect may also be indirectly analyzed by surface roughness measurements which is further discussed in section 5.2.

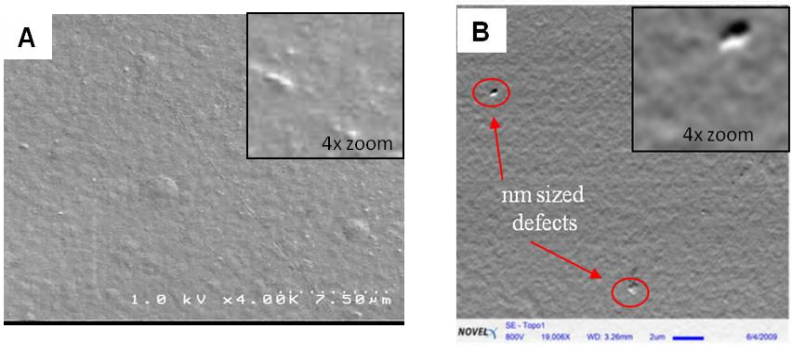

Figure 26: A) SEM imaging shows no evidence of sub-micron sized pinholes. B) Higher resolution imaging by a low voltage, quad-detectors mySEM® (with capability to show 3-D features) confirms no pinholes were detected on parylene films of ~1 µm thick.

Furthermore, parylene coating of 3um thickness was deposited to protect only the left half of PMMA mesh (Figure 27A), HARMS with AR=10 synthesized using LIGA with walls between hexagons measuring 1500 um tall and 150 um wide. Acetone is a known organic solvent that strongly affects/dissolves PMMA and many other polymers[27]; therefore, the whole mesh is soaked in an acetone bath for the duration of 2.5 hours, and the result is documented with a camera. As can be seen in Figure 27B, the right unprotected half of PMMA mesh walls was completely dissolved. However, the other half of the mesh protected by parylene coating was intact and no visual defects or damages including pinholes caused by acetone to PMMA at room temperature below the parylene coating were observed in the camera image (Figure 27B) thus further confirming pinhole-free Parylene-C coating on PMMA and most likely true for several other polymers. Higher resolution SEM imaging, conducted for closer inspection of

the interface of parylene-degraded PMMA surfaces (Figure 27C), shows PMMA sidewalls with wavy, rough features which are indication of degradation cause by acetone in parylene-free area of the mesh. In the same image, no surface damages are observed on the chemically inert parylene coating that is protecting the underlying PMMA.

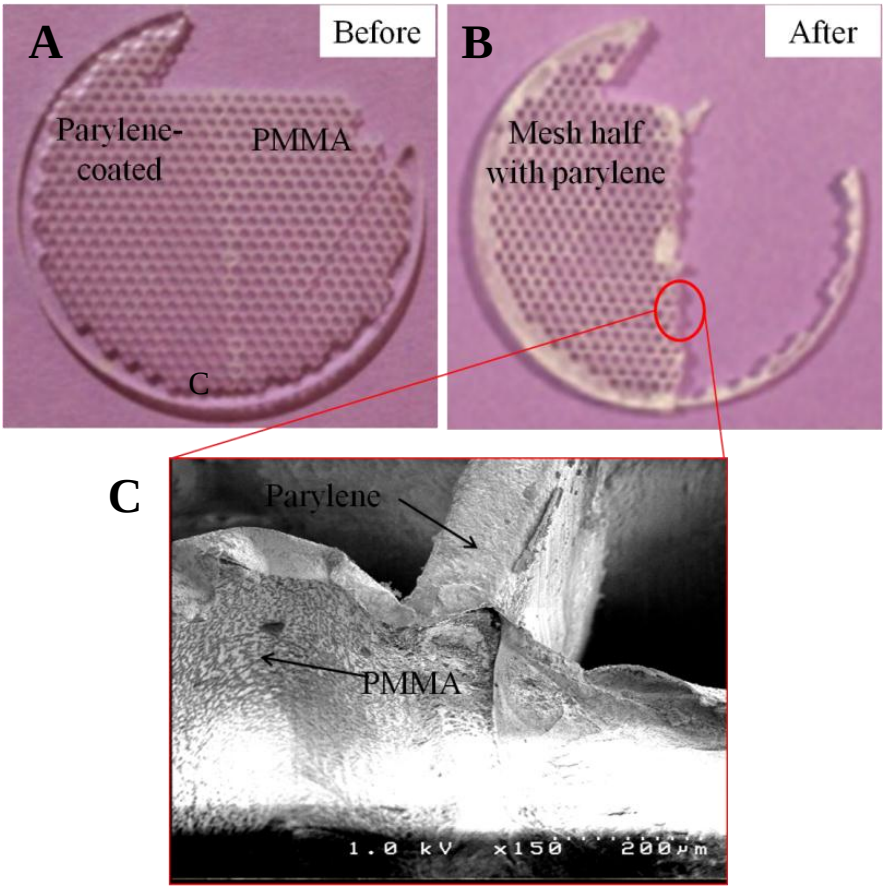

Figure 27: A) PMMA mesh was coated with 3 um thickness parylene and was soaked in acetone for 2.5 hours. B) The non-coated areas were completely dissolved by acetone. C) SEM showing no damage to parylene and the underneath PMMA after extended exposure to acetone.

5.2 Surface Roughness

Surface roughness were investigated on Ni HARMS (AR>10), PMMA microstructures (depth 200µm and width 600µm), and flat non-structured PMMA and PC surfaces deposited with parylene of 3µm thickness. Initially, qualitative observation of the SEM micrographs (Figure 28A) shows porous, pebble-like features with sizes of a few hundred nanometers on electroplated nickel surface, and a more

uniformly leveled surface with less number of pebble-like features are observe after parylene deposition (Figure 28B). Similarly, machining marks, sizes of low microns, on the embossing mold insert transferred into the PMMA surface (Figure 28C) are qualitatively observed to smoothed out after parylene deposition (Figure 28D). The smoothed out of surfaces may results from rounding effects induced by the growing thickness of the coating. An example of rounding effect is illustrated in Figure 29, where parylene deposition process would initially conformably coats the features everywhere (Figure 29B) and continue to grows and close the gap between the channel (Figure 29C) until the coating thickness gets large enough that the spacing between the features are connected and the edges are smoothen (Figure 29D). Therefore, rounding can affects the surface roughness on the nickel and PMMA surfaces where parylene coating thickness of ~3um would cover and hide smaller features, thus explaining the qualitative observation of reduction in surface roughness after parylene deposition.

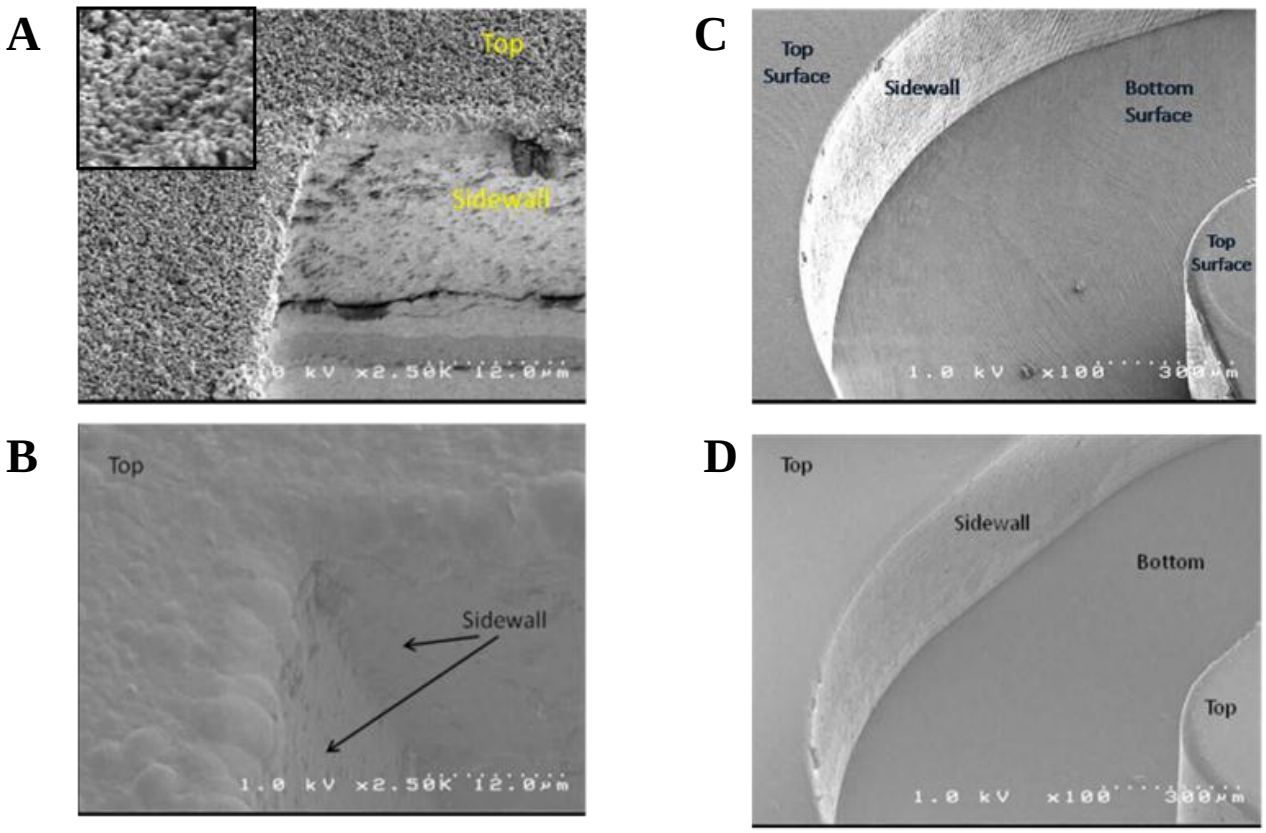

Figure 28: Reduction in roughness is observed for Ni HARMS before (A) and after (B) coating. Similar findings are seen before (C) and after (D) on PMMA HARMS.

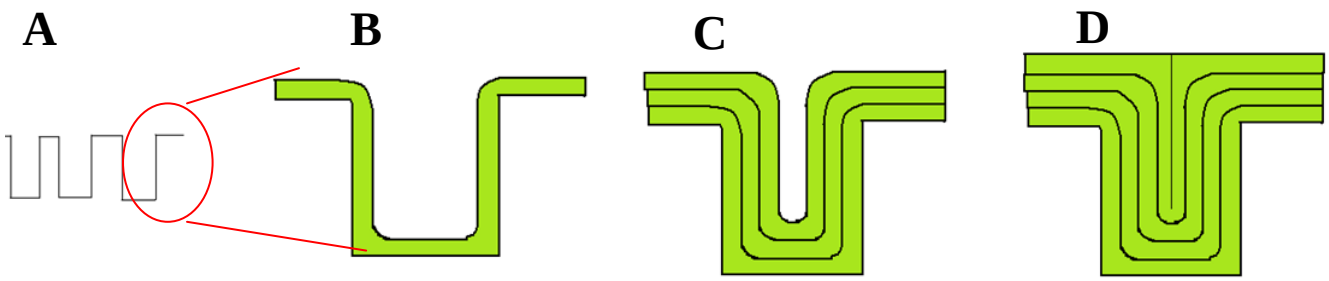

Figure 29: Illustration explaining rounding effects. A) Example of rough surface. B) Parylene initially conformably coats the surfaces of the feature with minimal rounding effect. C) The coating continue to grow and reduce the distance between valley until D) parylene completely fills the spacing and smooth out the edges.

The quantitative measurements of these surface roughnesses were performed using optical profilometry technique and atomic force microscopy. Figure 30 shows that electroplated Ni substrates with HARMS, which were used to deposit 3µm thick parylene, were observed to be very rough with average surface roughness (R_a) of 374 $\pm$ 42nm. Parylene deposition on these substrates resulted into decreasing the roughness to nearly half to 201 $\pm$ 24nm. Roughness measurements were also performed on pristine PMMA and polycarbonate surfaces and roughness of these surfaces remain relatively unchanged as pristine PMMA has average roughness of 2.66$\pm$0.35nm and after parylene deposition, it hardly changes to 2.85$\pm$0.6nm and pristine polycarbonate has average roughness of 3.02$\pm$0.31nm before and barely changes afterwards to 5.92$\pm$0.45nm. The roughness measurements indicate that parylene coating thickness of 3um or greater reduces roughness on electroplated Ni surfaces which has features of a few hundred nanometers while flat PMMA and PC surfaces are minimally affected. These quantitative results support the qualitative reduction in roughness seen in section 5.1.

The usage of adhesion promoter to enhance adhesion of parylene to sample surfaces changes the surface profile and roughness (Figure 31 and 32). When the vapor form of the adhesion promoter A174NT was used, the formation of "bubble" features was prominently observed on PMMA surfaces (Figure 31B). The "bubble" features most likely formed during the pre-parylene preparation stage where adhesion promoter, liquid A174NT, is vaporize (200-320°C) and enters the parylene deposition chamber

(room temperature) and settles on the samples. This process takes upwards to 3 hours to complete, and most likely during this time that the adhesion promoter vapors begins accumulating on the sample surfaces and pooled into droplets thus forming "bubble" features. Afterwards, these features are preserved by the conformable deposition of parylene, which the SEM images in Figure 32 clearly shown. The roughness values when adhesion promoter in combination of 14µm thick coating increases more than 20-fold from average roughness (R_q) of 63.22±5nm (Figure 31A) to 1300 ±421nm (Figure 31B). Similar changes to roughness were also observed on polycarbonate surfaces as the average roughness increase from 243±26nm to 1300±340nm, after using adhesion promoter.

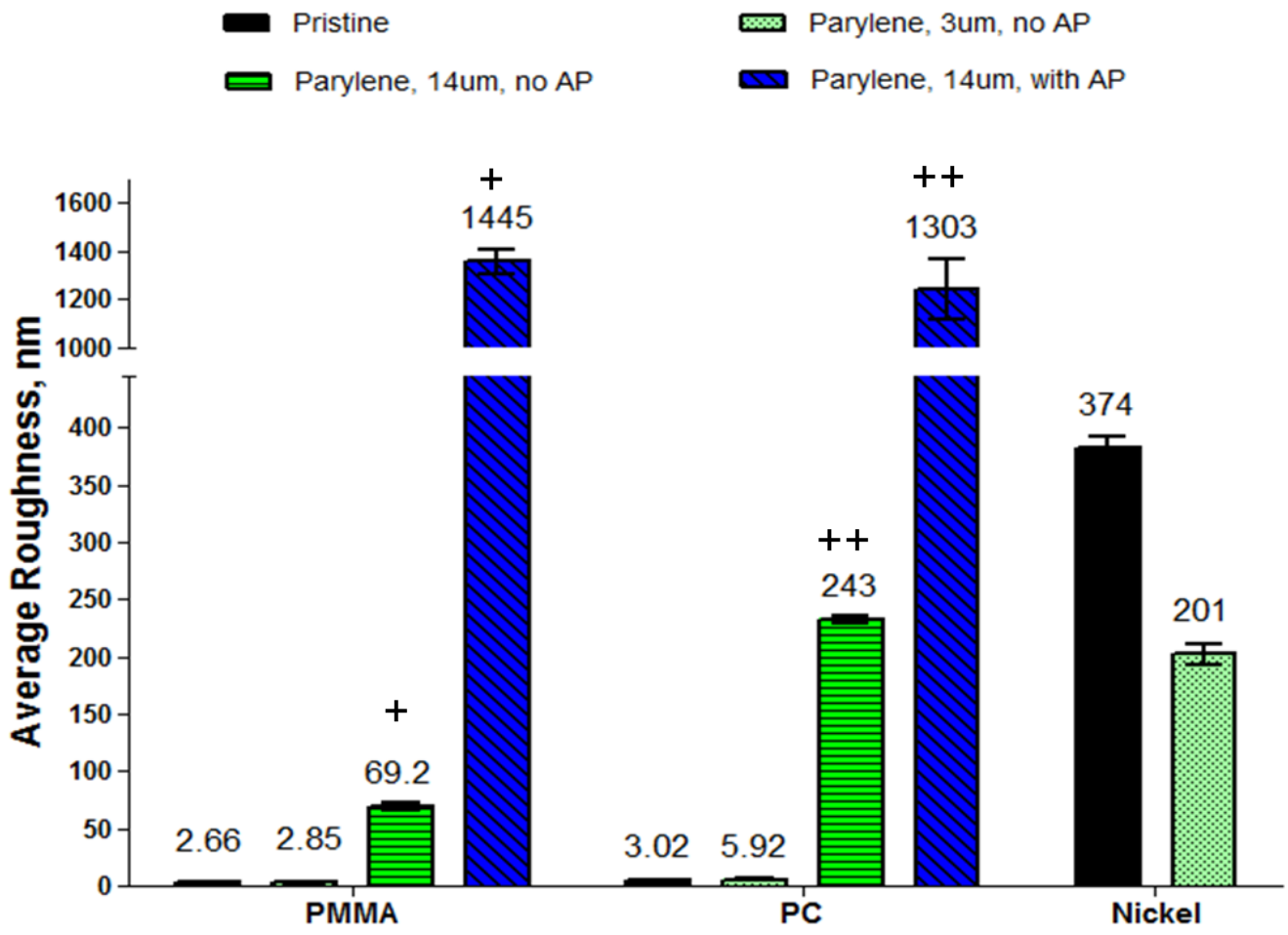

Figure 30: Optical profilometry results showing surface roughness values for PMMA, PC and nickel surfaces before and after parylene deposition. Roughness increases by several order of magnitude between PMMA (+) and PC (++) surfaces before and after 14um deposition with and without adhesion promoter.

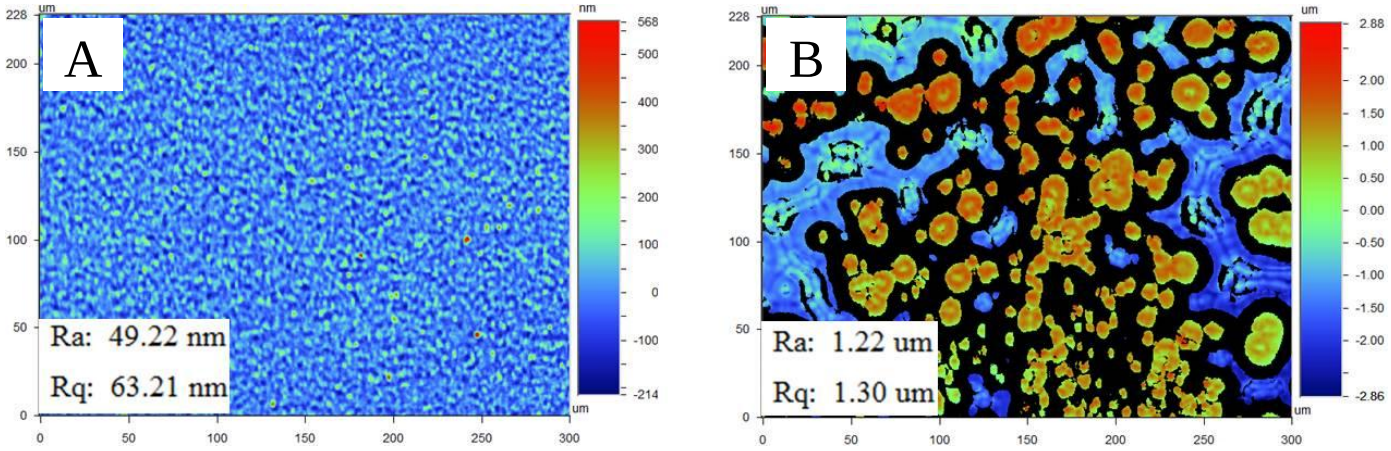

Figure 31: Optical profiler images showing polycarbonate surfaces before (left) and "bubble" features observed when using adhesion promoter (right).

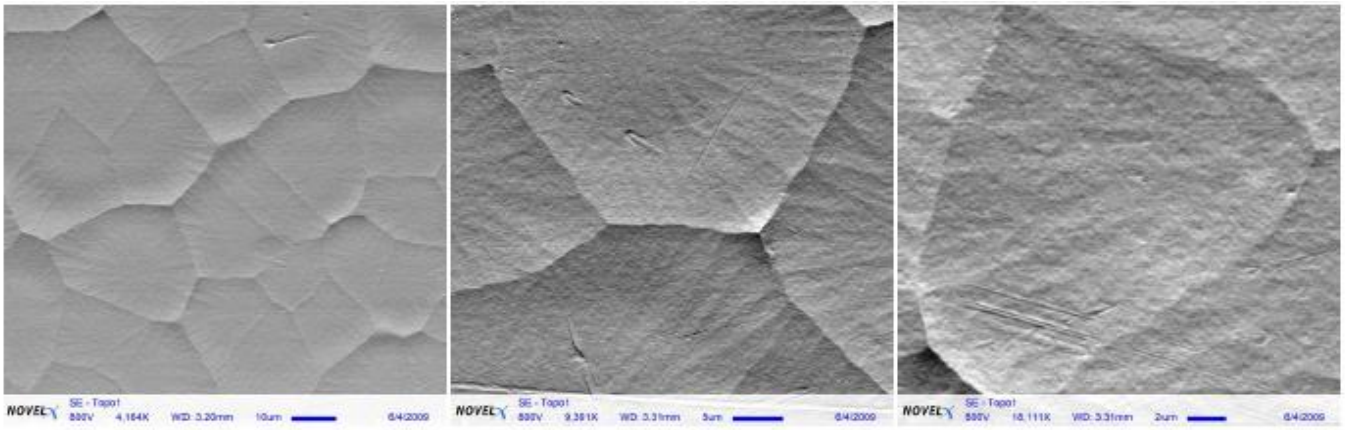

Figure 32: MySEM imaging of parylene deposition using adhesion promoter on polymer surfaces. Dimple-like features observed are likely due to non-uniform dispersion of adhesion promoter, A174-NT.

In addition to changing surface roughness using adhesion promoter, it can also be modified physically, Figure 33. Using fine sandpaper (800 grit size), we were able to increase roughness of flat PMMA surfaces from average roughness of 2.66±0.35nm to 250nm ± 6.4nm. The subsequent deposition of 1µm thick parylene did not significantly ($p>0.05$, t-test) alter the roughness with values slightly increasing to 261nm ± 6.9nm. The non-significant change in roughness is most likely because of rounding effect as described in section 5.2 by the 1µm thick coating depositing over nanometer roughness. Using rougher sandpaper (600 grit size) yielded the same result trend as PMMA surface were modified to have roughness of 824nm ± 48nm (using 600 grit size sand paper) before deposition and 822nm ± 2nm after coating with parylene.

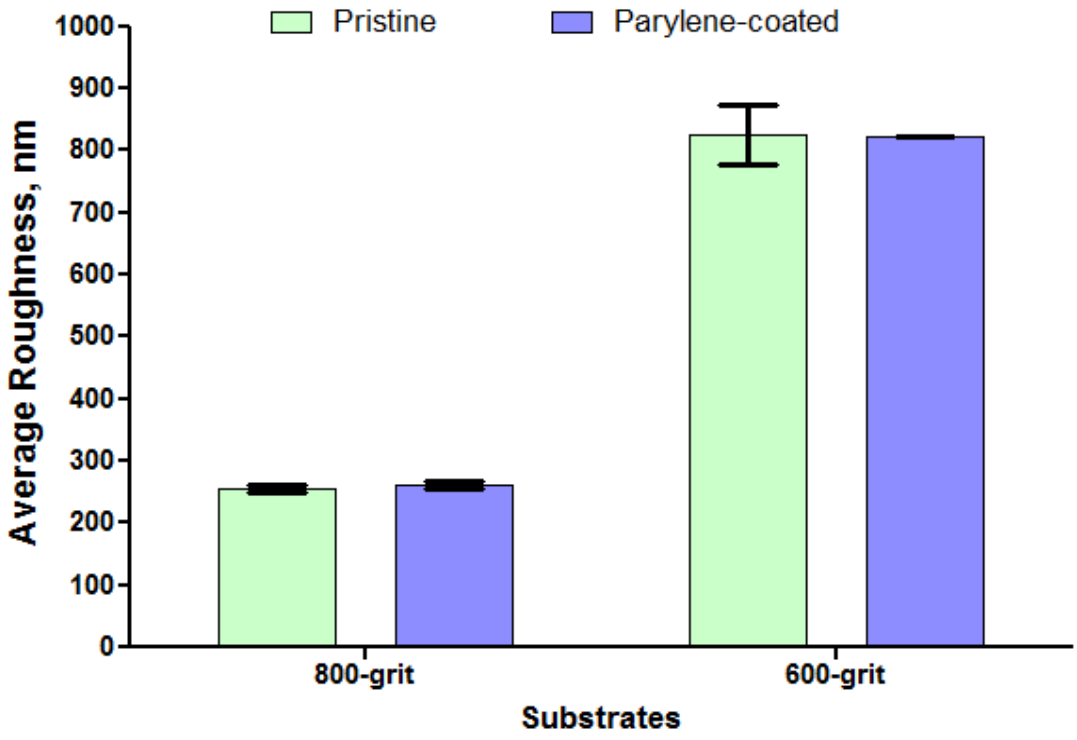

Figure 33: Physically alteration of surface roughness of PMMA using different grit sandpapers. Data obtained by Martina Cihova (CAMD Summer Internship 2010) [28]

5.3 Surface Modifications

Surface modification is a method for tailoring of surfaces to increase functionality. Initially, the surface roughness of the samples, pristine and after surface modification, was quantified using optical profiler. The methods employed to modify these surfaces were RF based oxygen plasma, ethanol (EtOH), and manually roughening the substrate surface before deposition of parylene. As seen in Figure 34, the average roughness values obtained from optical profiler for PMMA (R_a=2.69nm$\pm$0.62nm, PC (R_a=2.92nm$\pm$0.86nm), and parylene (R_a=4.61nm$\pm$0.78nm) were relatively unchanged after surface modification. This may be due to limitation in the lateral spatial resolution (x-y plane, ~200nm) of an optical microscope according to Abbe Principle [29] to detect nano-size changes, as surface roughness of PMMA and PC substrates after exposure to both plasma and ethanol are expected to alter since these two treatments are known to etch away polymer [12, 30].

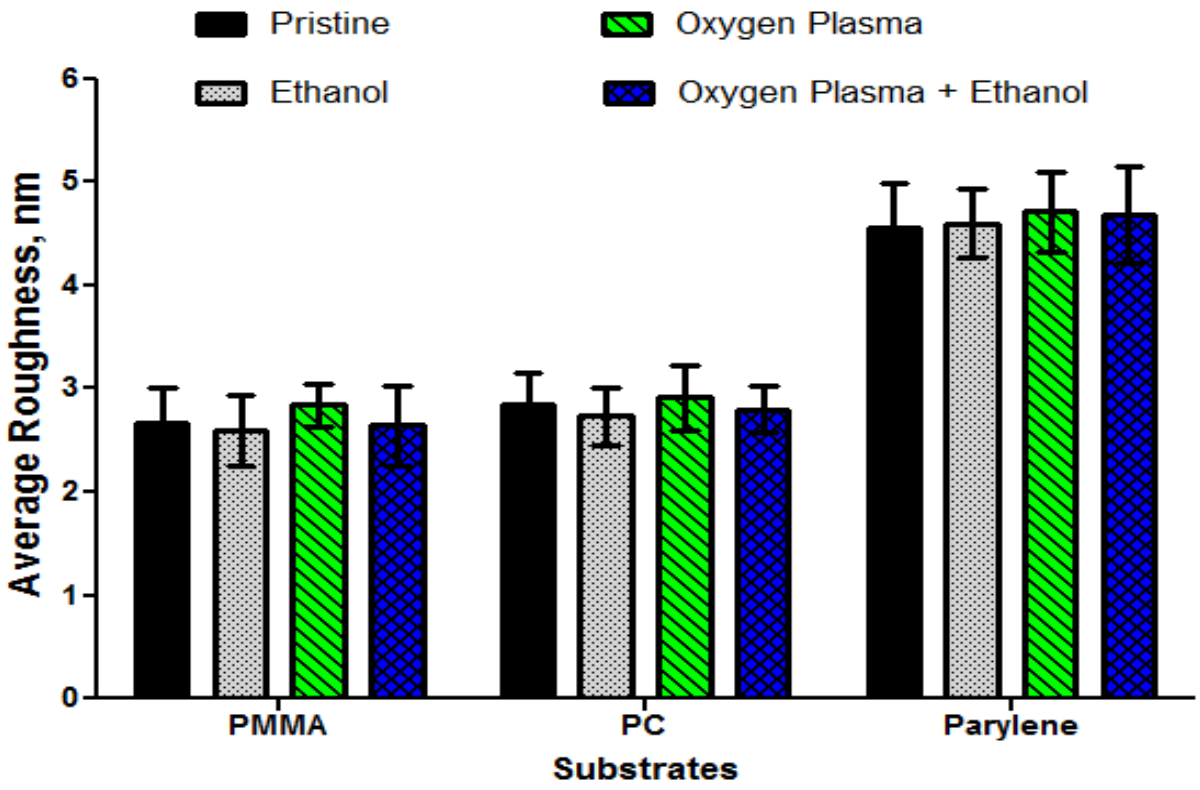

Figure 34: Optical profiler roughness measurement results on modified polymeric surfaces. Relatively no changes are observed to polymer surfaces with respect to treatment with ethanol, O_2 plasma, and combination of ethanol and O_2 plasma.

Atomic force microscopy (AFM), which is known to have spatial resolution down to one nanometer, is used to further investigate the impact of plasma/EtOH on surface roughness (due to etching) especially the creation of nanometer-sized features. Initially, AFM measurement within 50um scan area (Figure 35) were attain for bulk material surface analysis and the results shows pristine PMMA average roughness reduces from 8.92nm$\pm$1.3nm to 4.79nm$\pm$2.1nm after exposure to combination of plasma and ethanol. Pristine polycarbonate (R_a= 9.5nm$\pm$1.87nm) shows slight reduction in roughness after oxygen plasma (R_a=8.2nm$\pm$2.82nm) and combination of both plasma and ethanol (R_a=5.9nm$\pm$1.94nm). Parylene-coated samples show similar reducing trend with pristine parylene have average roughness of 12.1nm$\pm$3.72nm and decreases to average roughness of 6.4nm$\pm$0.83nm after being treated with plasma and ethanol. The minimal reduction in surface roughness is most likely due to ethanol and oxygen plasma

affecting only the nano-sized top surface layer of the bulk material. The result is more consistent with other studies[12, 23, 27] which have shown the etching effect of plasma and ethanol on polymers on reducing nanometer surface roughness.

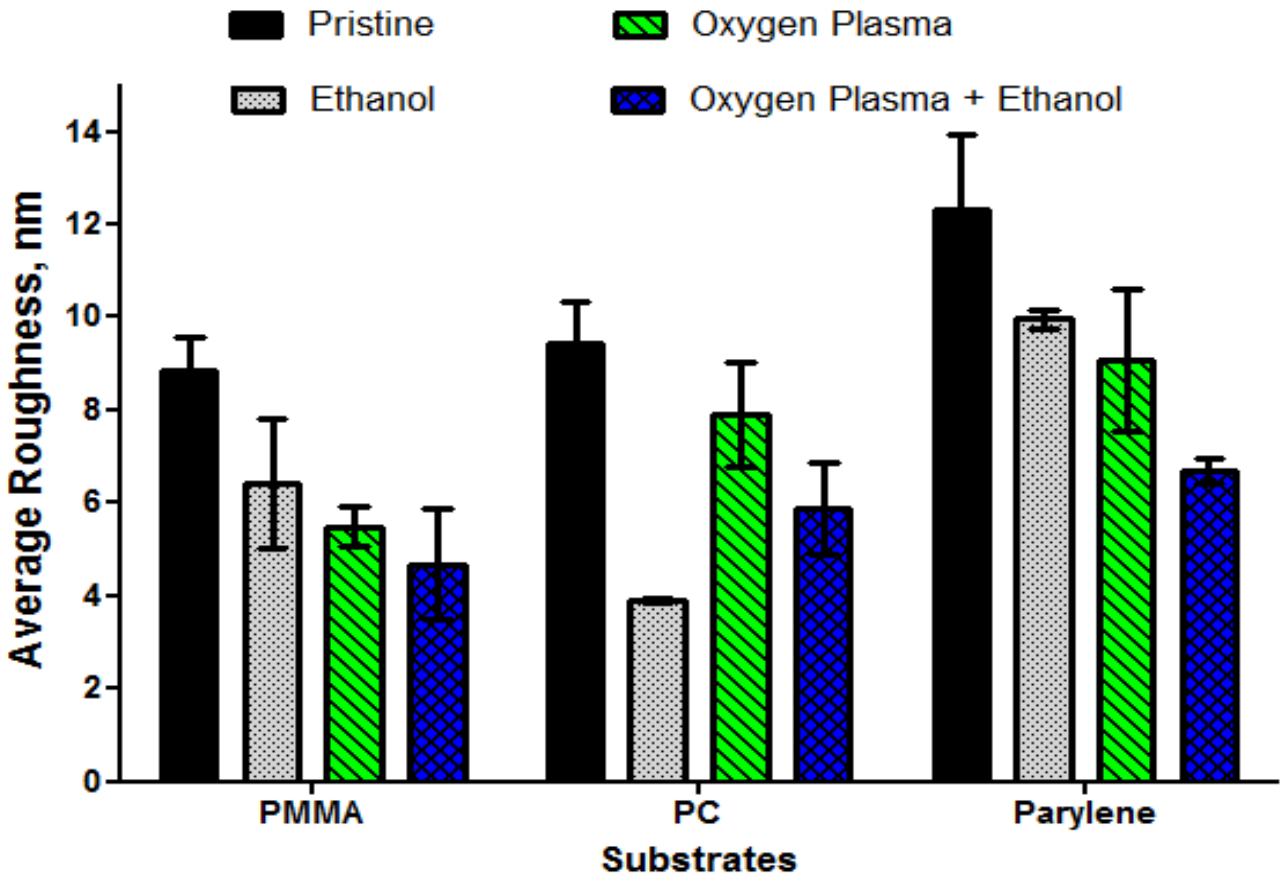

Figure 35: AFM roughness measurement within 50µm by 50µm scan area showing results on modified polymeric surfaces. Surface roughness is slightly reduced for samples treated with ethanol. Combination of oxygen plasma and ethanol causes higher reduction of surface roughness.

AFM measurements were also taken within 5µm x 5µm scan area for higher resolution analysis of the surface (Figure 36). The result exhibits a similar reducing trend of surface roughness after surface modification. Average surface roughness for the different samples were also within nanometers range (<13nm) which are similar to measurements obtained from the 50µm by 50µm AFM scan area and optical profiler results. This means that for most applications where a few nanometers roughness are not as important, optical profiler results are adequate as obtaining data using AFM can be time consuming.

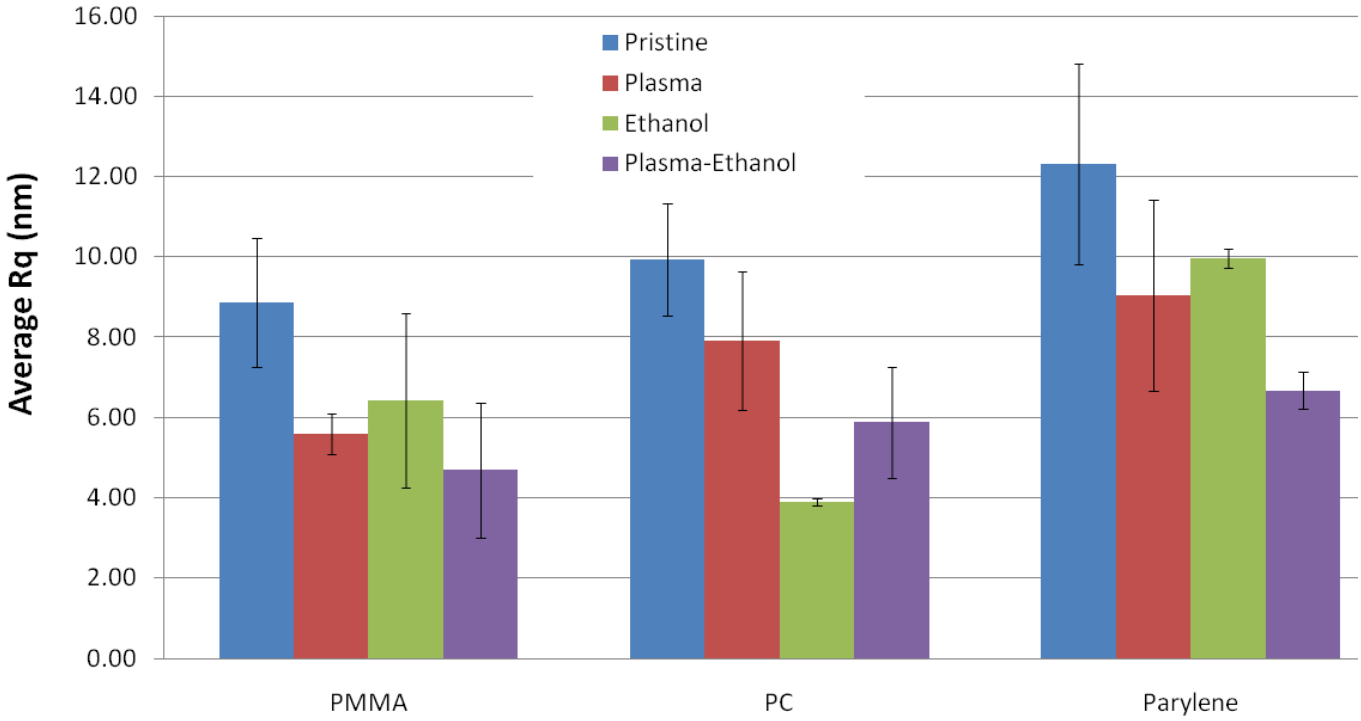

Figure 36: AFM measurement values within 5µm x 5µm scan area.

Since surface modification using ethanol and oxygen have been shown to affect surface roughness, contact angle was measured to investigate the changes to surface energy resulting from the modifications as surface hydrophobicity and roughness are important factors influencing cell adhesion6. Static contact angle were first measured on pristine, flat surfaces of PMMA, PC, and parylene and then compared to oxygen plasma-treated and EtOH exposed surfaces to observe changes (Figure 37 and Table 3). The average contact angle of pristine PMMA, PC, and parylene-C substrates were ~65°, ~73°, and ~89°, respectively. These values are similar to those reported from other studies6,[31]. Reductions in contact angle are observed throughout all O_2 plasma-treated surfaces. This finding concurs with previous finding6 and most likely due to the formation of hydroxyl groups from the O_2 plasma process[12]. On the other hand, ethanol exposed surfaces were observed to have increased contact angle; therefore, relative increase in hydrophobicity. This is probably due to formation of carbonyl groups forming on the surfaces as result of reaction with ethanol[31].

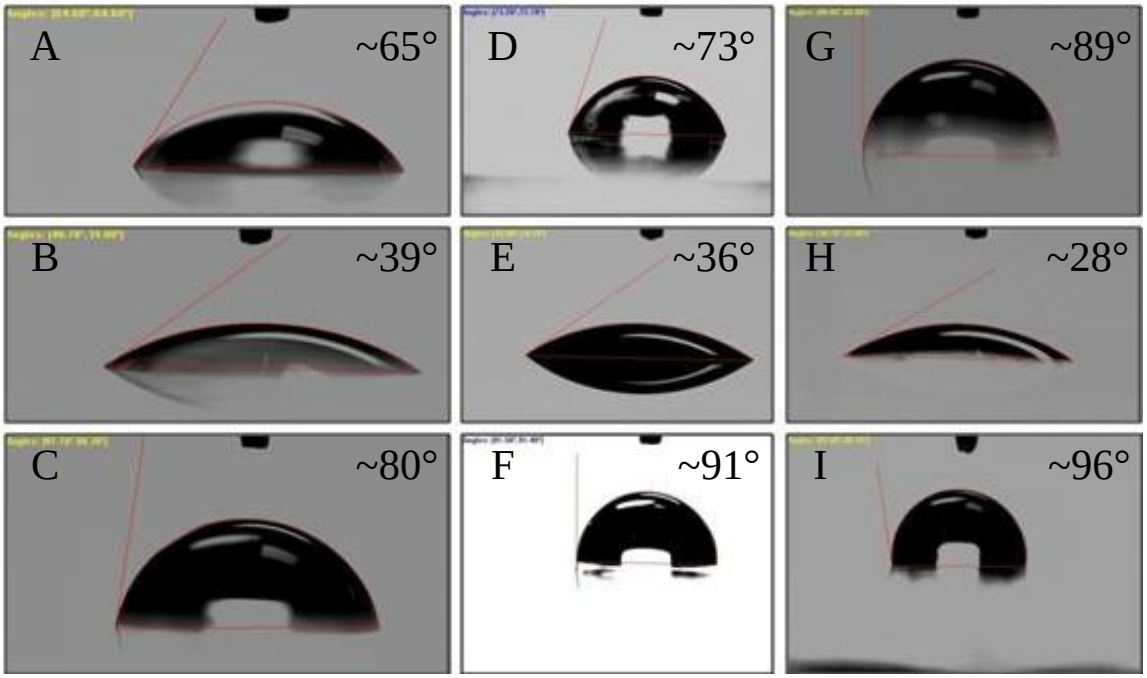

Figure 37. Contact angle images of PMMA, PC, and parylene surfaces before and after surface modification. A) Pristine PMMA, B) Oxygen plasma modified PMMA, C) Ethanol modified PMMA, D) pristine PC, E) oxygen plasma modified PC, F) ethanol modified PC, G) pristine parylene, H) oxygen plasma modified parylene, and I) ethanol modified parylene.

Table 3: Contact angle measurements of PMMA, PC, and parylene surfaces before and after surface modification.

	Contact angle (degrees)			
Substrates	**Untreated**	**Plasma-treated**	**EtOH exposed**	**Plasma/EtOH**
PMMA	65.2 ± 1.16	39.7 ± 3.08	79.9 ± 3.09	80.2 ± 1.54
PC	72.9 ± 1.06	36.3 ± 3.43	91.1 ± 1.70	77.4 ± 3.86
Parylene	89.2 ± 1.09	28.4 ± 2.50	96.5 ± 1.82	66.6 ± 2.78

Further, contact angle was measured to investigate the duration and storage environments of parylene samples after modifying with oxygen plasma since time between surface modification and biological cells study can be several hours apart and at different location. During the duration study, O_2 plasma treated parylene surfaces were enclosed within plastic bags which were stored in the open atmosphere, dry nitrogen (N_2), and under vacuum ($\leq 10^{-5}$ torr) to study the effects of these environment on the plasma treated surfaces. Figure 38 shows that after 3 hours, the contact angles were similar for all

three environments (~30°). After 101 hours, samples kept in vacuum are measured to be at 40° which is lower than CA than those in open atmosphere (52°) and N_2 (53°). These results indicate that oxygen plasma modified parylene surfaces are constantly changing whereby oxygen plasma initially decreases the contact angle or increase the surface energy. High energy surface attracts particles and/or impurities in the atmosphere to settle down on the surface which causes the surface energy to decrease and contact angle to increase. Since vacuum has significantly much lower quantity of particles and/or impurities, their deposition on the surface is much less. Further, most of the changes observed may be mainly due to particles/impurities depositing during the time between plasma processing and transferring of sample to vacuum and during the period where samples are taken from the vacuum chamber and carried to the contact angle measurement site. This study shows similar results to Chang *et al* (2007)[23] that contact angles do not remain constant but steadily increases over time. Chang *et al* (2007)[23] observed oxygen plasma treated parylene deposited on silicon remains hydrophilic (4.4±2.4 degrees) and did not revert to hydrophobic 40 minutes after treatment.

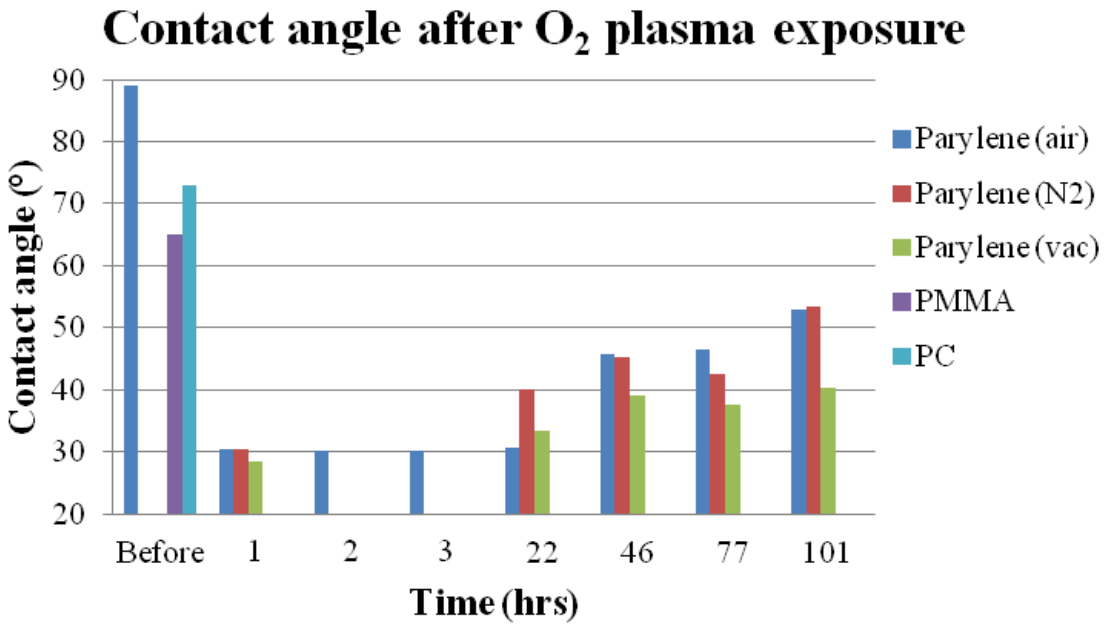

Figure 38: Chart summarizing the study on the effect duration of O_2 plasma treatment on parylene surfaces.

The formations of hydroxyl and carbonyl due to oxygen plasma and ethanol discussed earlier were studies conducted on PMMA; however, these effects were not studied on parylene. A preliminary study was setup to investigate if the same effects are observed with parylene. Fourier-Transform Infrared Spectroscopy (FTIR), a technique used to analyze formations and degradation of chemical bonds was utilized. Figure 39 shows C=C absorbance peak values at 1500cm^{-1} and C-H bonds at ranges 2850-3100cm^{-2} and 1370-1430cm^{-1}.

These peaks are expected as parylene's molecular structure is an aromatic benzene ring. Hydroxyl bonds, peaks within ranges of 3100-3500cm^{-1} and 2500-2800cm^{-1}, were not observed in the FTIR spectra. It is most likely that surface modification only affects the few layers on top of the surface (few nanometers thickness) whereas FTIR is a bulk analysis technique. FTIR signal received is from entire 1µm thick parylene and the chemical changes on the top surface probably do not produce enough signals to be detected. In order to increase the effect of oxygen plasma, 1um thick parylene film was treated with oxygen plasma and then successively folded over 10 times. Peaks for hydroxyl bonds (3100-3500cm^{-1} and 2500-2800cm^{-1}) were still not observed (Figure 39). Therefore, in order to confirm the surface chemistry change, a more surface sensitive technique like X-ray photoelectron spectroscopy (XPS) is required.

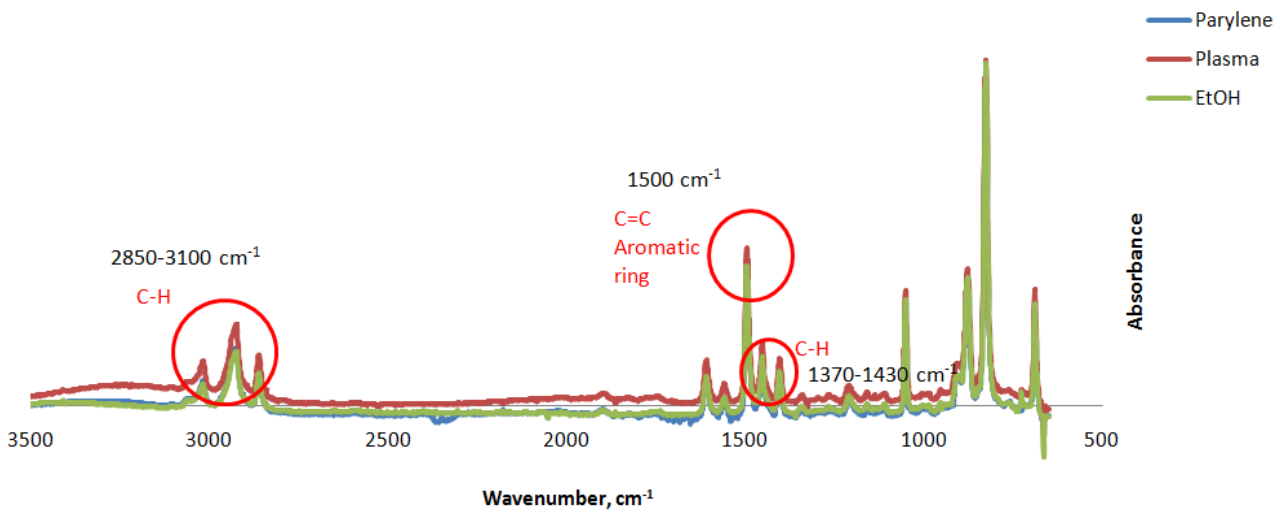

Figure 39: FTIR spectra showing similar absorbance peaks for three different parylene surfaces.

5.4 Cell Adhesion

In order to evaluate the biocompatibility of parylene-C coated substrates relative to PMMA and PC, cell adhesion and spreading of HeLa epithelial cells were intially analyzed using optical microscopy (Figure 40). Observation of brightfield images (Figure 40) shows little or no effect of plasma treatment on cell adhesion on PMMA and PC substrates. In addition, PC surfaces have qualitatively greater cell adhesion and spreading than PMMA surfaces. However, parylene-C surfaces have the most difference in the number of cell adhering before and after O_2 plasma treatment. It was observed that the least amount of cell adhesion and spreading are seen on untreated parylene-C surfaces, and the number greatly increased with O_2 plasma treatment. The promotion of cells to adhere to O_2 plasma modified surfaces is very useful in BioMEMS application whereby selective modification of parylene in the reaction or detection chamber with oxygen plasma will greatly promote cell adhesion and increase signal output while reducing cell agglomeration in non-modified surfaces like microfluidic channels. The results are similar to those reported by Chang *et al* (2007)[23] in that surface modification of Parylene-C surfaces using O_2 plasma promotes the adhesion of fibroblast and hepatocyte cells. The observations are best described after 24 hours of incubation.

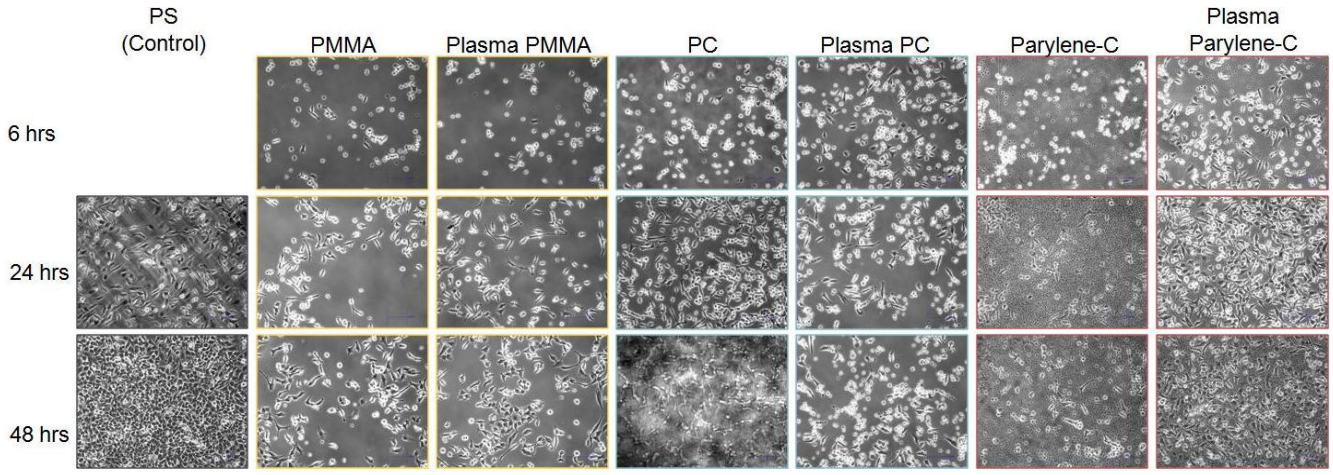

Figure 40: Brightfield images taken showing cell adhesion and spreading. Non-adherent cells remain in spherical shape while adherent cells elongate and spread on the surfaces. Parylene-C surfaces show the lowest cell adhesion (untreated) and highest cell adhesion (plasma-treated). Images were taken at 6, 24, and 48 hours.

Study of cell adhesion was also conducted on surfaces with tailored roughness obtained by physically roughening them.. Flat PMMA surfaces were initially polished with different grit size paper and subsequently coated with 1µm thick parylene and surface roughness of a few hundred nanometers up to over a micron were obtained as presented in section 5.2. In Figure 41, cell adhesion results shows a few HeLa cells (~10-100µm) attaching to very smooth surfaces (R_a=2.85nm$\pm$0.6nm) (Figure 41A) and the number slight increased for surfaces with average roughness of 250nm$\pm$6.4nm (Figure 41B), which is similar to findings of increase smooth muscle cells adhesion on ~368nm rough surface reported by Haberstroh *et al* (2003)[32]. On surfaces with average roughness 824nm$\pm$28nm (Figure 37C) and just over one micron, little to no cell adhesion are observed. Since cells adhesion is determined by the interactions of proteins/ligands found in the extracelluar matrix (ECM)[33] and the material surface, and that HeLa cells are ~10µm while in suspension, the contacting surface area of the ECM to the surface may be higher for average roughness ~250nm (Figure 42A) than surface with greater roughness (Figure 42B). Figure 42 also demonstrate that types of surface roughness (rods, hemi-spherical, cylindrical, etc) may also affect the contact area of ECM. Although higher surface roughness may provide greater surface area for cells to attach, the range of roughness, the surface roughness profiles, and surface chemistry are more influential factors for cell adhesion.

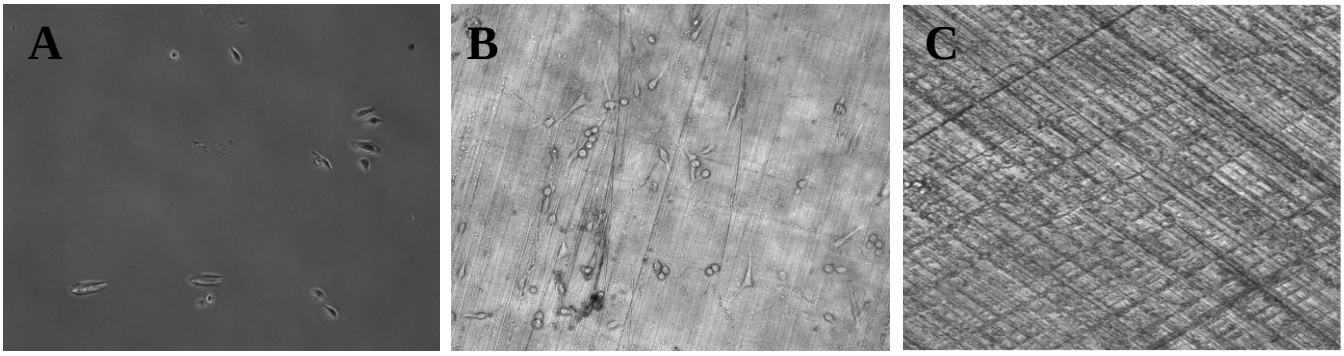

Figure 41: HeLa cells attaching surfaces of roughness approximately A) 2.85nm, B) 250nm and C) 800nm. Images taken by Martina Cihova (CAMD Summer Internship 2010)[28]

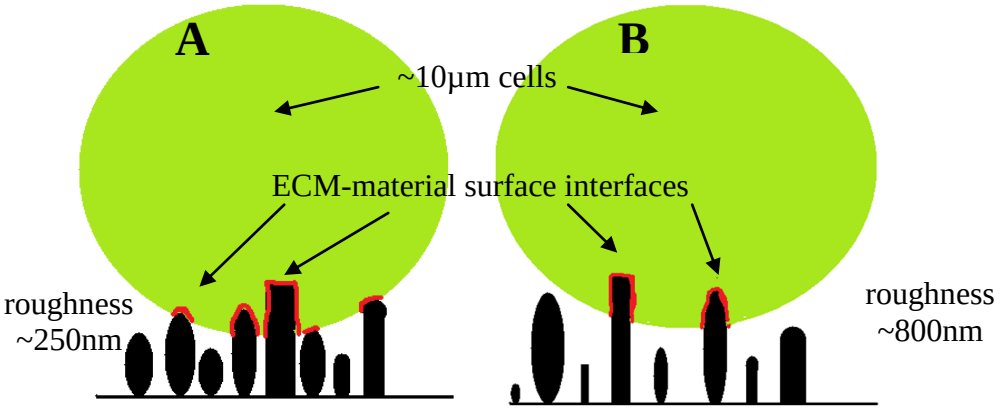

Figure 42: An illustation describing cells adhesion on different ranges and types of roughness. A) Average roughness ~250nm with rods, cylinders, hemi-spheres, etc. features. B) Average roughness ~800nm with rods, cylinders, hemi-spheres, etc. features. The red outlines indicate contact area between extracellular matrix and material surface.

In addition to brightfield imaging, fluorescent techniques were also used to characterize parylene surfaces. In Figure 43A, fluorescent images show HeLa cells adhering and spreading across the polystyrene surface (standard material in cell culture). The same cell behaviors are also observed on parylene surface (Figure 43B and C) which demonstrates that the surface is compatible with respect to HeLa cells. Furthermore, fluorescence analysis using Calcein AM, which is uptake and hydrolyze into calcein by only live cells, demonstrated that parylene surfaces are not cytotoxic to HeLa cells which are similar to other studies[6, 7]. Although parylene is non-toxic, cell adhesion between pristine and oxygen plasma modified surfaces were qualitatively observed to be different as greater number of cells adhering to O_2 plasma modified parylene surface (Figure 43C) than pristine surface (Figure 43B).

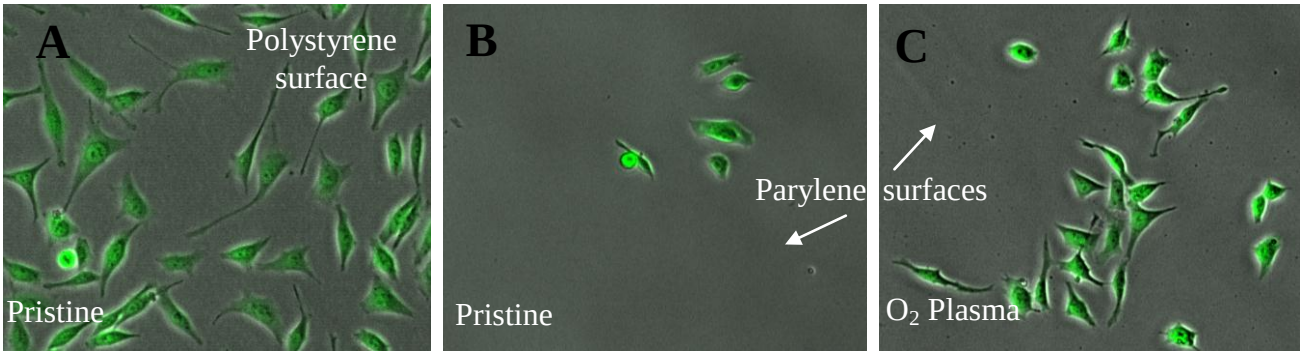

Figure 43: HeLa cells stained with fluorescent live-cell dye calcein on A) non-treated cell culture dish, B) pristine Parylene-C, and C) oxygen plasma modified parylene-C. The cells were incubated on the surface for 48 hours.

Quantification of cell numbers was investigated in order to examine the extent of the promotion of cells resulting from surface modification. Initially, quantification of cell adhesion was conducted by using a fluorescence microscope to image cells stained with calcein within the field of view of a 10X objective. The number of cells on the image was manually counted and the results (Figure 44) show increases in cell adhesion to all surfaces after oxygen plasma treatment. PMMA has almost a 50% increase from 28 cells to 55 cells while PC surfaces show a 28.5% increase from 69 cells to 90 cells. Parylene surfaces have the highest increase in term of percentage from 7 cells to 38 cells after O_2 plasma treatment which is over a 500% cell promotion. However, manual counting is not an efficient method as quantification of large pool of data is very time consuming. Therefore, automated counting using ImageJ software was tested to see if it is a viable alternative. A graph comparing manual versus automated counting is shown in Figure 45. The number of cells counted using ImageJ on all surfaces was on average less than 20% lower than the manual count. The automated counting also yields the same trend as manual counting. This means that automated counting is a viable option for rapid processing of cell quantification in cell adhesion study.

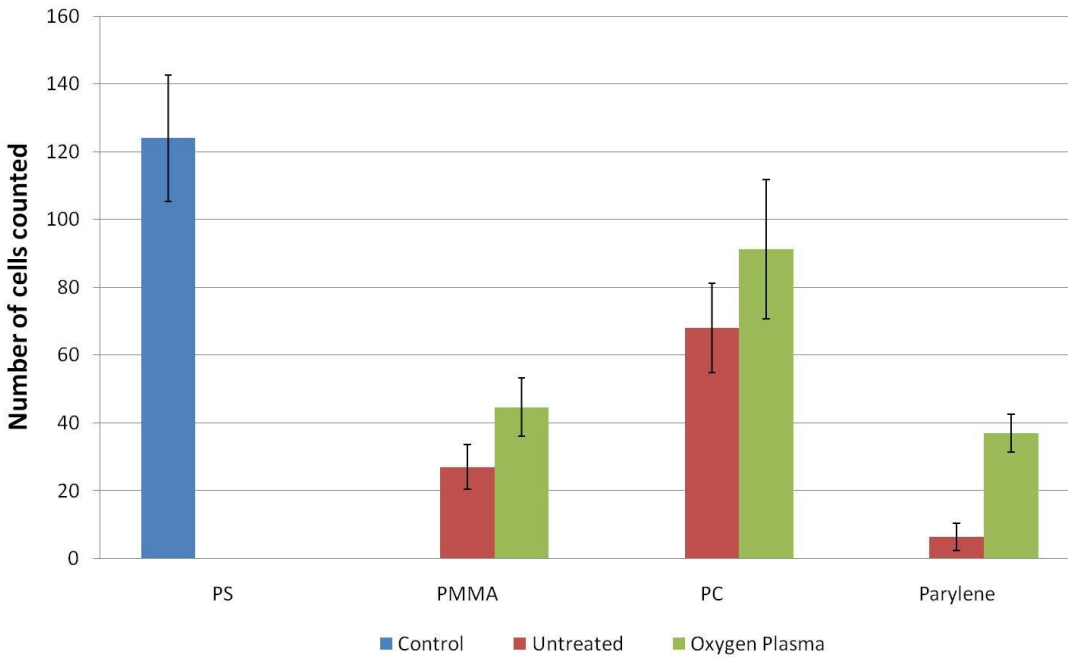

Figure 44: Manual count of the number of HeLa cells adhering to PMMA, PC, and Parylene-C surfaces. Major increases in cell adhesion are counted on Parylene-C surface after O_2 plasma treatment.

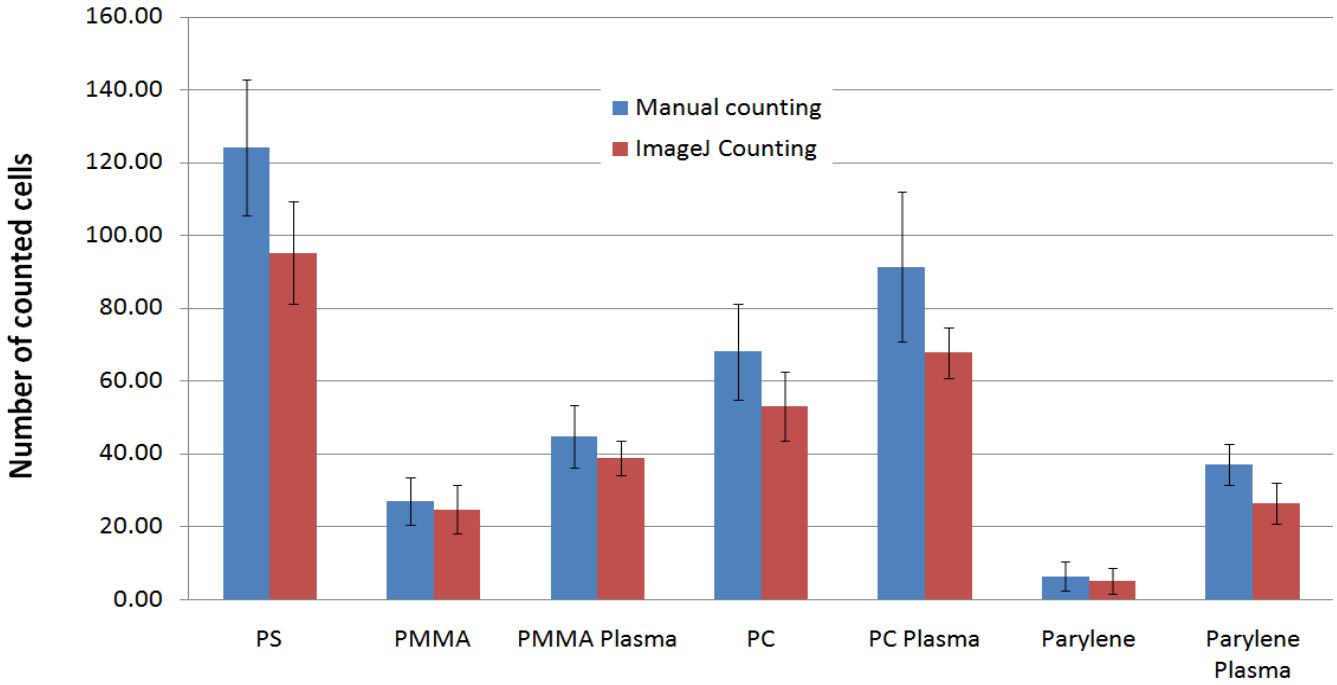

Figure 45: Chart showing the number of HeLa cells counted manually and by imageJ software.

Quantification using calcein staining in combination with fluorescent imaging is an acceptable initial evaluation of cell adhesion; however, the field of view of the microscope and its objective lenses limits the study to describe cell activity only in localize areas. In order to gain a better understand of cell attachment and dispersion across the entire substrate's surface, a more comprehensive quantitative study is needed. AlamarBlue®, as detailed in section 4.5, is a cell health indicator assay that measure cellular activities of an entire surface. Since cell's metabolic activities are only active after it has adhered to a surface and begin spreading, alamarBlue® can measures these activities and indirectly be use to quantify cell adhesion. The graph in Figure 46 details the number of cells adhering to surfaces after 18 hours of incubation time. The result is similar to Calcein assay. Pristine parylene has the lowest number of cell adhering to the surface with 7744 $\pm$ 322 cells out of initially 20,000 cells. The number of adherent cells significantly ($p>0.05$, t-test) increases to 18510 $\pm$ 1576 cells which are greater than a two-fold increase with modification using oxygen plasma. A greater number of cells, 21485 $\pm$ 2731, were seen on O_2 plasma plus 75% EtOH treated samples but the results were not significant ($p>0.05$, t-test). Cell number

for O_2 plasma plus ethanol modified surface exceed the initial seeding of 20,000 cells because there is at least a 10-15% error when counting with a haemocytometer. The cell adhesion results are similar to those observed by Chang et al (2007)[23]. The authors' results show at least 70-folds increase in cell adhesion for AML-12 hepatocyte and a 2-folds increase for NIH-3T3 fibroblast between pristine and oxygen plasma modified parylene surfaces. This study results and the findings reported by Chang *et* al (2007)[23] demonstrated that the magnitude of the promotion of cell adhesion on oxygen plasma modified surfaces can vary differently between cell line which may interact differently with the surfaces due to chemistry and/or surface roughness. In addition, the oxygen plasma technique, equipment use to treat the surfaces, and other parameters may also be different.

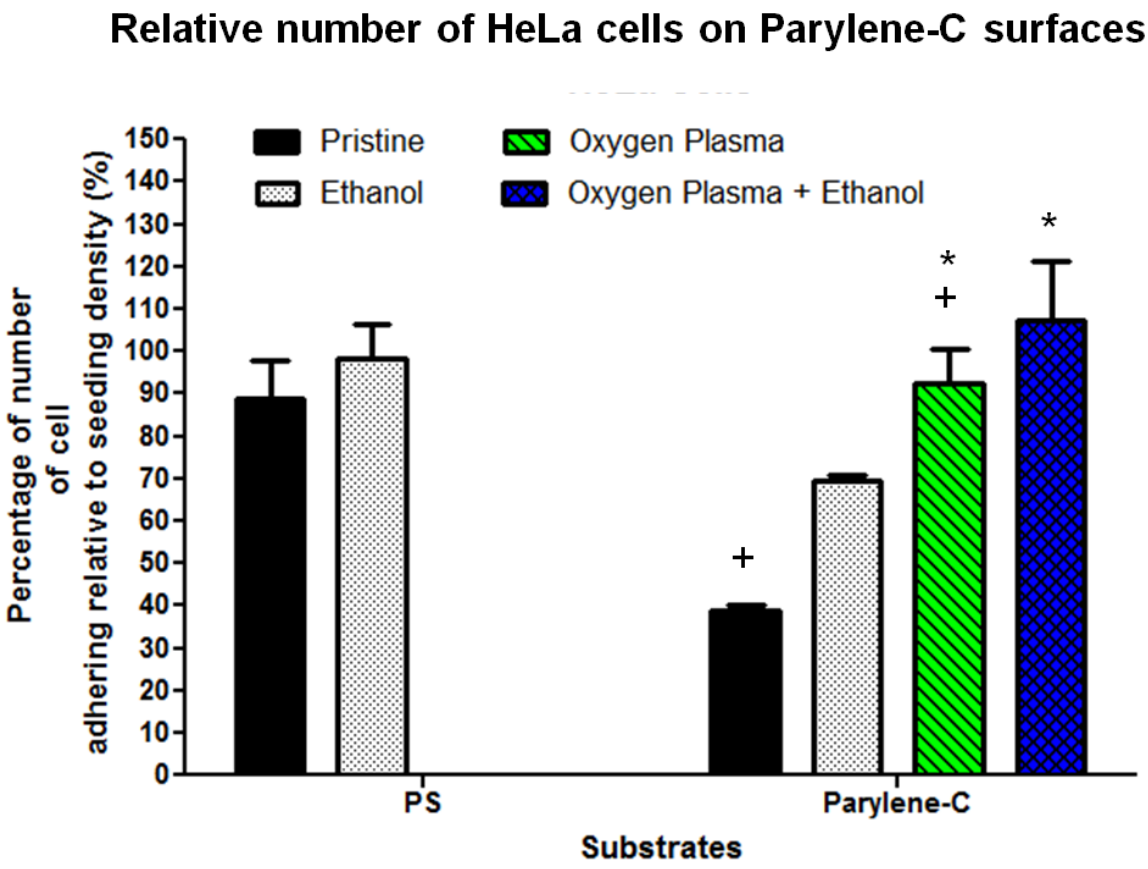

Figure 46: Percentage of the number of cells adhering to pristine and modified parylene surfaces. The (+) denotes significant difference ($p<0.05$) between pristine and oxygen plasma treated parylene-C surface (t-test). The (*) denotes no significant difference ($P>0.05$) between oxygen plasma and oxygen plasma plus 75% ethanol treated parylene-C surfaces (t-test).

5.5 BioMEMs Applications

Molding requires rigid molds fabricated from rigid materials such as silicon, brass, nickel, or even polymers. However, the adhesion between the mold materials and the molded polymeric structure is often a damaging factor, especially when molding HARMs. Parylene is known for possessing lower coefficient of friction (COF=0.29) and high melting temperature (T=290°C) than molded materials and its study as a re-usable hot embossing mold master for producing mold insert has also been reported[21]. We proposed to test parylene as a releasing layer in the molding process. Firstly, PMMA sheets were coated with 12 um thick layer of parylene-C. Then, a brass mold insert (Figure 47A) with HARMs were embossed onto parylene coated PMMA surface. Qualitatively, it was easier to remove the brass mold insert from the parylene-coated PMMA sheets than from regular PMMA sheets. This is most likely due to the lower COF of parylene which reduces sticking to brass mold insert. We also investigate the condition of the parylene skin after embossing. Parylene remains intact on flat surface of HARMs. However, the parylene encompassing edges and sidewalls of the microstructures was compromised. This is most likely due to high shearing forces experienced by parylene during embossing and/ or not enough thickness of parylene coating which lead to tearing of the coating. Coating parylene on the mold insert as oppose to the PMMA may be a much better option.

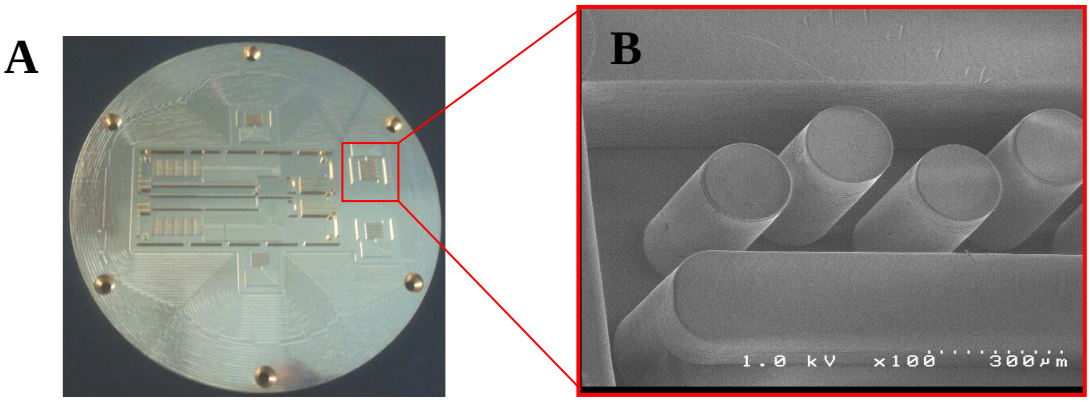

Figure 47: A) Brass mold insert with HARMs. B) Magnify SEM image of replicated HARMs on PMMA using mold insert.

The conformal deposition of parylene also enables it to be an excellent coating material for controlling thickness of devices which require precise dimensional controls. For examples, Figure 48 shows SEM images of SU8 microstructures with hexagonal pore sizes in the order of ~60um in diameter (Figure 48A) and after several controlled deposition, the pore size can be reduced by a number of microns to ~31um (Figure 48B) and even further down to ~20um (Figure 48C). Thinner, more control deposition of parylene is also possible. Figure 48D shows a circular design with initial pore size in the order of ~13um. Subsequent deposition reduces the pore size ~1.5um per deposition to ~11.5um (Figure 48E) and ~10um (Figure 48F). The results show that the thickness of parylene (Figure 49) can be used to control the hole size as per requirements set by various bio-filter applications.

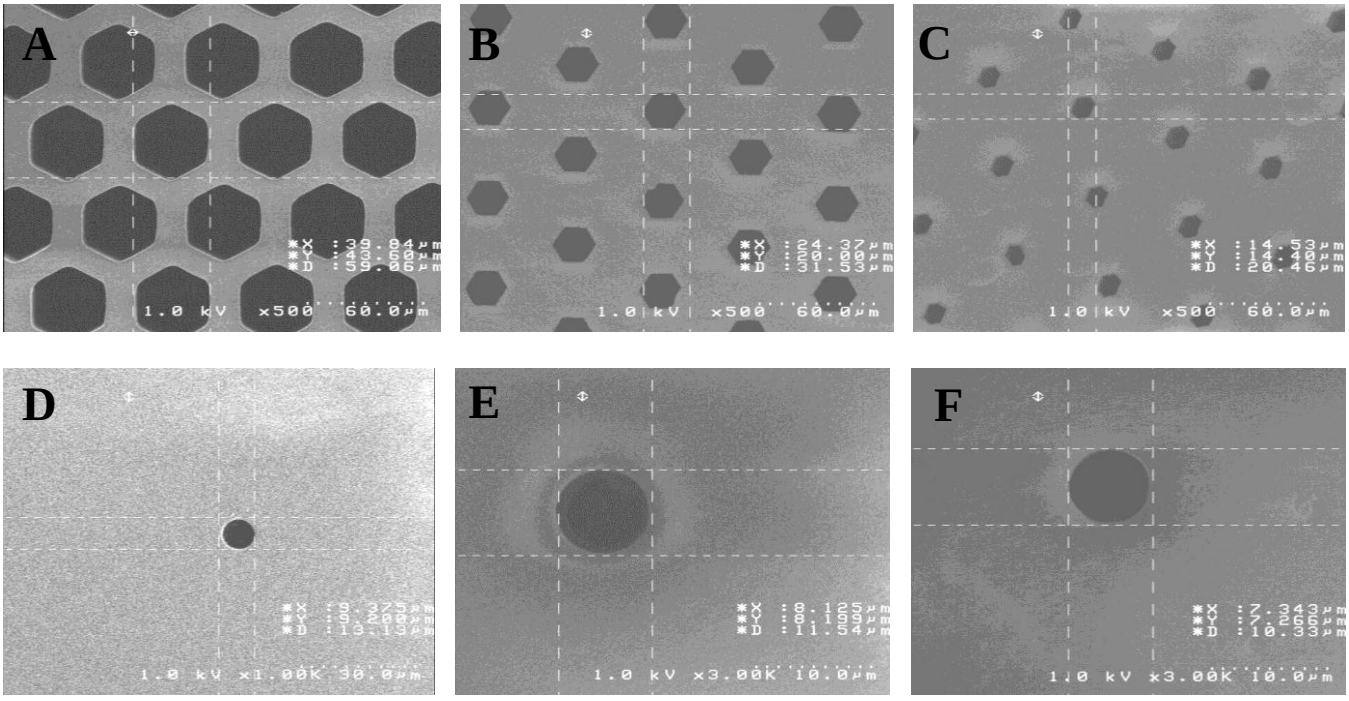

Figure 48: SEM images showing controlled controllable parylene deposition for tailoring pore sizes in bio-filter devices. Hexagonal pores: (A) no parylene ~60um, (B) parylene deposition ~31um, and (C) parylene deposition ~20.5 um. Circular pores: (D) no parylene ~13um, (E) 1st deposition reduces by ~1.5um, (F) 2nd deposition reduces by ~1.5um.

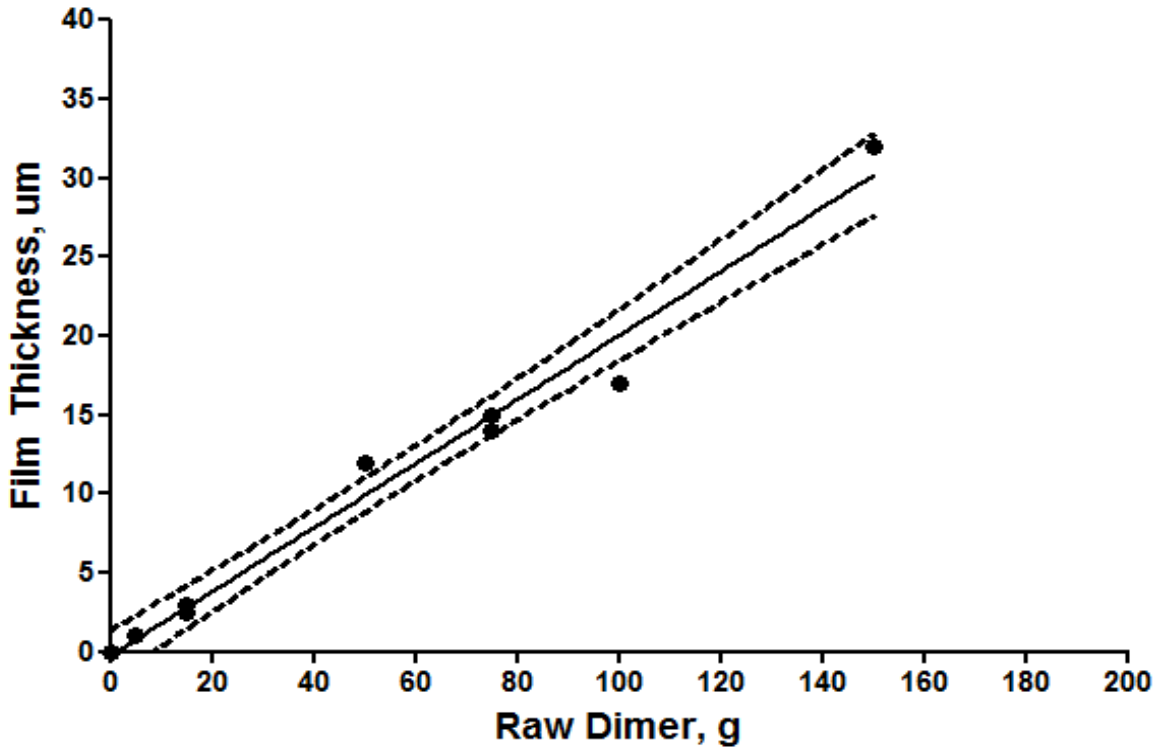

Figure 49: Graph showing direct correlation of parylene film thickness to raw dimer used. Dotted lines showed 95% confidence interval.

CHAPTER 6: CONCLUSIONS

In this study, parylene-C was demonstrated to be conformably deposited on microfluidic structures with aspect ratios as high as over 10 with thickness down to 1um and no pinhole $\leq$100nm were observed. These show that parylene is suitable for both normal and HAR microfluidic designs and that it is pinhole-free with respect to cellular applications. Additionally, the surface roughness ia "tailorable" for parylene surface as ~1-3μm thick deposition of parylene can mimic the roughness of the intended substrate or increase by a few magnitude with the help of an adhesion promoter and coating of higher thickness. This is advantageous as roughness is one factor affecting cell adhesion. This study also has shown surface modification using O_2 plasma, its effects on surface roughness and energy, and subsequently cell adhesion. The contact angle of pristine parylene surface changes from 89° to 28° after O_2 plasma treatment. Parylene-C has also shown to be non-cytotoxic and that pristine Parylene-C yielded the least cell adhesion. This is advantageous for bio-devices as pristine parylene will reduce the chances of cell agglomeration within microfluidic channels which lead to clogging. On the other hand, surface modification using O_2 plasma promotes HeLa cell adhesions by at least 2-fold which can be implemented on areas of bio-devices such as reaction chamber to increase the capturing of cells. Overall, the parylene-C has been shown to a suitable biocompatible coating for BioMEMS applications due to its tailorable surface as well as its conformability.

REFERENCES

[1] Haeberle, S. and R. Zengerle (2007). "Microfluidic platforms for lab-on-a-chip applications." Lab on a Chip **7**(9): 1094-1110.

[2] "E.p.t® Digital Pregnancy Test | E.p.t®." *E.p.t® | The Accuracy You Want, When You Need It the Most.* Web. 31 Oct. 2011. <http://www.errorprooftest.com/products/digital>.

[3] "Bedside Blood Analysis | Handheld Blood Analyzer | Abbott Point of Care.com." *I-STAT® System | Point-of-Care Testing | Handheld Blood Analyzer | Abbott Point of Care.com*. Web. 31 Oct. 2011. <http://www.abbottpointofcare.com/Products-and-Services.aspx>.

[4] Derek Brown, Microfluidic Device for Diagnostic Analysis of Human Body Fluid. HARMST Poster 2009.

[5] Becker, H. and U. Heim (2000). "Hot embossing as a method for the fabrication of polymer high aspect ratio structures." Sensors and Actuators a-Physical **83**(1-3): 130-135.

[6] Chang, T. Y., V. G. Yadav, et al. (2007). "Cell and protein compatibility of parylene-C surfaces." Langmuir **23**(23): 11718-11725.

[7] Feili, D., M. Schuettler, et al. (2005). "Encapsulation of organic field effect transistors for flexible biomedical microimplants." Sensors and Actuators a-Physical **120**(1): 101-109.

[8] Ehrfeld, W., V. Hessel, et al. (1998). "Microreactors for chemical synthesis and biotechnology - Current developments and future applications." Microsystem Technology in Chemistry and Life Science **194**: 233-252.

[9] Simpson, P. C., D. Roach, et al. (1998). "High-throughput genetic analysis using microfabricated 96-sample capillary array electrophoresis microplates." Proceedings of the National Academy of Sciences of the United States of America **95**(5): 2256-2261.

[10] Jackman, R. J., D. C. Duffy, et al. (1998). "Fabricating large arrays of microwells with arbitrary dimensions and filling them using discontinuous dewetting." Analytical Chemistry **70**(11): 2280-2287.

[11] Kim, K., S. Park, et al. (2002). "Rapid replication of polymeric and metallic high aspect ratio microstructures using PDMS and LIGA technology." Microsystem Technologies **9**(1-2): 5-10.

[12] Meng, E., P. Y. Li, et al. (2008). "Plasma removal of parylene c." Journal of Micromechanics and Microengineering **18**(4): -.

[13] Fortin, Jeffery and Toh-Ming Lu. Chemical Vapor Deposition Polymerization: The Growth and Properties of Parylene Thin Films. Boston: Kluwer Academic Publishers, 2004.

[14] "PARYLENE KNOWLEDGE." *The Parylene Leader - Specialty Coating Systems*. Web. 07 Nov. 2011. <http://www.scscoatings.com/parylene_knowledge/index.aspx>.
[15] Beach, William F. (1978). "A Model for Vapor Deposition Polymerization of *p*-Xylylene." Macromolecules **11**(1): 72-76.

[16] Haberstroh, K. M., A. Thapa, et al. (2003). "Nano-structured polymers enhance bladder smooth muscle cell function." Biomaterials **24**(17): 2915-2926.

[17] Khang, D., S. Y. Kim, et al. (2007). "Enhanced fibronectin adsorption on carbon nanotube/poly(carbonate) urethane: Independent role of surface nano-roughness and associated surface energy." Biomaterials **28**(32): 4756-4768.

[18] Noh, H. S., Y. Huang, et al. (2004). "Parylene micromolding, a rapid and low-cost fabrication method for parylene microchannel." Sensors and Actuators B-Chemical **102**(1): 78-85.

[19] Deguchi, K., N. Takeuchi, et al. (2002). "Evaluation of pressure uniformity using a pressure-sensitive film and calculation of wafer distortions caused by mold press in imprint lithography." Japanese Journal of Applied Physics Part 1-Regular Papers Short Notes & Review Papers **41**(6B): 4178-4181.

[20] Scheer, H. C. and H. Schulz (2001). "A contribution to the flow behaviour of thin polymer films during hot embossing lithography." Microelectronic Engineering **56**(3-4): 311-332.

[21] Youn, S. W., H. Goto, et al. (2007). "Fabrication of a micro patterned parylene-C master by hot-embossing and its application to metallic mold replication." Journal of Micromechanics and Microengineering **17**(7): 1402-1413.

[22] Kroschwitz, J.I., ed. Kirk-othmer Encyclopedia of Chemical Technology, John Wiley & Sons, Inc.: New York, 1998.

[23] Chang, T. Y., V. G. Yadav, et al. (2007). "Cell and protein compatibility of parylene-C surfaces." Langmuir **23**(23): 11718-11725.

[24] Wright, D., B. Rajalingam, et al. (2008). "Reusable, reversibly sealable parylene membranes for cell and protein patterning." Journal of Biomedical Materials Research Part A **85A**(2): 530-538.

[25] Ilic, B., H.G. Craighead (2000). "Topographical Patterning of Chemically Sensitive Biological Materials Using a Polymer-Based Dry Lift Off." Biomedical Devices **2**(4): 317-322.

[26] Atsuta, K., H. Suzuki, et al. (2007). "A parylene lift-off process with microfluidic channels for selective protein patterning." Journal of Micromechanics and Microengineering **17**(3): 496-500.

[27] Zhou, X. D., S. C. Zhang, et al. (2001). "Effect of the solvent on the particle morphology of spray dried PMMA." Journal of Materials Science **36**(15): 3759-3768.

[28] Martina Cihova. CAMD Summer Intership Program (2010).

[29] Hell, S. W. (2003). "Toward fluorescence nanoscopy." Nature Biotechnology **21**(11): 1347-1355.

[30] Ibnabddjalil, M., I. H. Loh, et al. (1994). "Effect of Surface Plasma Treatment on the Chemical, Physical, Morphological, and Mechanical-Properties of Totally Absorbable Bone Internal-Fixation Devices." Journal of Biomedical Materials Research **28**(3): 289-301.

[31] Henry, A. C., T. J. Tutt, et al. (2000). "Surface modification of poly(methyl methacrylate) used in the fabrication of microanalytical devices." Analytical Chemistry **72**(21): 5331-5337.

[32] Thapa, A., D. C. Miller, et al. (2003). "Nano-structured polymers enhance bladder smooth muscle cell function." Biomaterials **24**(17): 2915-2926.

[33] Boudreau, N. and M. J. Bissell (1998). "Extracellular matrix signaling: integration of form and function in normal and malignant cells." Current Opinion in Cell Biology **10**(5): 640-646.

VITA

Quoc Phuc Nguyen was born in Long An, Viet Nam on October 20, 1984. At the age of 8 he immigrated to the United States of America and attended Eaton Park Elementary School in Abbeville, Louisiana, and two years later move to Erath, Louisiana. He graduated from Erath High School in May 2003 with the honorable title of valedictorian and continued his postsecondary education at Louisiana State University and obtained his Bachelor of Science in Bioengineering in May 2007. Quoc is currently pursuing a master's degree in Bioengineering under Dr. Varshni Singh and hopes to complete by December 2011.